REPORT DOCUMENTATION PAGE

Form Approved OMB No. 074-0188

1. AGENCY USE ONLY (Leave blank)	2. REPORT DATE	3. REPORT TYPE AND DATES COVERED
	April, 1998	

4. TITLE AND SUBTITLE
Laser Ablation/Ionization Characterization of Solids: Final Progress Report of the Strategic Environmental Research and Development Program

5. FUNDING NUMBERS
N/A

6. AUTHOR(S)
W.P. Hess, B.A. Bushaw, M.I. McCarthy, J.A. Campbell, S.D. Colson, J.T. Dickinson

7. PERFORMING ORGANIZATION NAME(S) AND ADDRESS(ES)
Pacific Northwest National Laboratory
PO Box 999
Richland, WA 99352

8. PERFORMING ORGANIZATION REPORT NUMBER
N/A

9. SPONSORING / MONITORING AGENCY NAME(S) AND ADDRESS(ES)
SERDP
901 North Stuart St. Suite 303
Arlington, VA 22203

10. SPONSORING / MONITORING AGENCY REPORT NUMBER
N/A

11. SUPPLEMENTARY NOTES
Pacific Northwest National Laboratory is operated for the US Department of Energy by Battell under Contract No. DE-AC06-76RLO 1830.

12a. DISTRIBUTION / AVAILABILITY STATEMENT
Approved for public release: distribution is unlimited.

12b. DISTRIBUTION CODE
A

13. ABSTRACT ***(Maximum 200 Words)***

The Department of Energy has undertaken the enormous task of remediating defense wastes and environmental insults which habe ocurred over 50 years of nuclear weapons production. It is abundantly clear that significant technology advances are needed to characterize, process, and store highly redioactive waste and to remediate contaminated zones. In addition to the processing and waste form issues, analytical technologies needed for the characterization of solids, and for monitoring storage tanks and contaminated sites do not exist or are currently expensive labor-intensive tasks. This report describes progress in developing sensitive, rapid, and widely applicable laser-based mass spectrometry techniques for analysis of mixed chemical wastes and contaminated soils.

The remediation of defense waste and the long-term disposal fo high-level mixed wastes requires chemical analysis of the waste streams. Efficient analytic methods are needed to characterize the chemical classes and concentrations of a wide variety of waste materials. Tank and crib waste sites contain broad distributions of radioisotopes, chelating agents, chromates, and ferrocyanides.

14. SUBJECT TERMS
LAMS; MALDI; REMPI; laser ablation; SERDP; SERDP Collection

15. NUMBER OF PAGES
51

16. PRICE CODE N/A

17. SECURITY CLASSIFICATION OF REPORT	18. SECURITY CLASSIFICATION OF THIS PAGE	19. SECURITY CLASSIFICATION OF ABSTRACT	20. LIMITATION OF ABSTRACT
unclass.	unclass.	unclass.	UL

REPORT DOCUMENTATION PAGE

Form Approved
OMB No. 074-0188

1. AGENCY USE ONLY (Leave blank)	2. REPORT DATE	3. REPORT TYPE AND DATES COVERED
	April, 1998	

4. TITLE AND SUBTITLE
Laser Ablation/Ionization Characterization of Solids: Final Progress Report of the Strategic Environmental Research and Development Program

5. FUNDING NUMBERS
N/A

6. AUTHOR(S)
W.P. Hess, B.A. Bushaw, M.I. McCarthy, J.A. Campbell, S.D. Colson, J.T. Dickinson

7. PERFORMING ORGANIZATION NAME(S) AND ADDRESS(ES)
Pacific Northwest National Laboratory
PO Box 999
Richland, WA 99352

8. PERFORMING ORGANIZATION REPORT NUMBER
N/A

9. SPONSORING / MONITORING AGENCY NAME(S) AND ADDRESS(ES)
SERDP
901 North Stuart St. Suite 303
Arlington, VA 22203

10. SPONSORING / MONITORING AGENCY REPORT NUMBER
N/A

11. SUPPLEMENTARY NOTES
Pacific Northwest National Laboratory is operated for the US Department of Energy by Battell under Contract No. DE-AC06-76RLO 1830.

12a. DISTRIBUTION / AVAILABILITY STATEMENT
Approved for public release: distribution is unlimited.

12b. DISTRIBUTION CODE
A

13. ABSTRACT ***(Maximum 200 Words)***

The Department of Energy has undertaken the enormous task of remediating defense wastes and environmental insults which habe ocurred over 50 years of nuclear weapons production. It is abundantly clear that significant technology advances are needed to characterize, process, and store highly redioactive waste and to remediate contaminated zones. In addition to the processing and waste form issues, analytical technologies needed for the characterization of solids, and for monitoring storage tanks and contaminated sites do not exist or are currently expensive labor-intensive tasks. This report describes progress in developing sensitive, rapid, and widely applicable laser-based mass spectrometry techniques for analysis of mixed chemical wastes and contaminated soils.

The remediation of defense waste and the long-term disposal fo high-level mixed wastes requires chemical analysis of the waste streams. Efficient analytic methods are needed to characterize the chemical classes and concentrations of a wide variety of waste materials. Tank and crib waste sites contain broad distributions of radioisotopes, chelating agents, chromates, and ferrocyanides.

14. SUBJECT TERMS
LAMS; MALDI; REMPI; laser ablation; SERDP; SERDP Collection

15. NUMBER OF PAGES
51

16. PRICE CODE N/A

17. SECURITY CLASSIFICATION OF REPORT	18. SECURITY CLASSIFICATION OF THIS PAGE	19. SECURITY CLASSIFICATION OF ABSTRACT	20. LIMITATION OF ABSTRACT
unclass.	unclass.	unclass.	UL

NSN 7540-01-280-5500

Standard Form 298 (Rev. 2-89)
Prescribed by ANSI Std. Z39-18
298-102

Laser Ablation/Ionization Characterization of Solids: Final Progress Report of the Strategic Environmental Research Development Program

by

W. P. Hess, B. A. Bushaw, M. I. McCarthy, J. A. Campbell, S. D. Colson

Pacific Northwet National Laboratory*
PO Box 999, Richland, WA 99352

and

J. T. Dickinson
Washington Statae University
Department of Physics
Pullman, WA 99164-2814 USA

*Pacific Northwest National Laboratory is operated for the U. S. Department of Energy by Battelle under Contract No. DE-AC06-76RLO 1830.

Table of Contents

Laser Ablation/Ionization Characterization of Solids: Final Progress Report to the Strategic Environmental Research Development Program

(April, 1998)

W. P. Hess, B. A. Bushaw, M. I. McCarthy, J. A. Campbell, S. D. Colson
Pacific Northwest National Laboratory
PO Box 999 Richland, WA 99352

J. T. Dickinson
Washington State University
Department of Physics
Pullman, WA 99164-2814 USA

I. INTRODUCTION

The Department of Energy has undertaken the enormous task of remediating defense wastes and environmental insults which have occurred over 50 years of nuclear weapons production. It is abundantly clear that significant technology advances are needed to characterize, process, and store highly radioactive waste and to remediate contaminated zones. In addition to the processing and waste form issues, analytical technologies needed for the characterization of solids, and for monitoring storage tanks and contaminated sites do not exist or are currently expensive labor-intensive tasks. This report describes progress in developing sensitive, rapid, and widely applicable laser-based mass spectrometry techniques for analysis of mixed chemical wastes and contaminated soils.

The remediation of defense waste and the long-term disposal of high-level mixed wastes requires chemical analysis of the waste streams. Efficient analytic methods are needed to characterize the chemical classes and concentrations of a wide variety of waste materials. Tank and crib waste sites contain broad distributions of radioisotopes, metals, TRU's, aromatic organic compounds, halogenated hydrocarbons, nitrates, chelating agents, chromates, and ferrocyanides. The chemical speciation and concentration of these materials must be determined in order to design effective clean-up strategies and to perform risk analysis. Additionally, the high concentrations of radioactive waste materials, in tanks and cribs, provide an energetic driving force that

continuously transforms mixed waste through complex kinetic pathways; hence, analyses need to be made in a timely fashion. Current methods require as much as six months to analyze a single waste tank core sample. This report outlines our initial efforts at developing rapid analysis techniques, which may be extended to on-line field measurements.

II. PROJECT DESCRIPTION

We are developing analysis techniques based on laser ablation mass spectroscopy (LAMS), matrix assisted laser desorption ionization (MALDI), and resonance enhanced multiple photon ionization (REMPI). Laser ablation is used to vaporize solid materials and the resulting pulsed plumes are analyzed using mass spectrometry or resonant laser ionization techniques. Analysis of even complex, multicomponent mixtures can be performed rapidly and requires very little sample. This is necessary for the analysis of many environmental samples and hazardous wastes. The concentrated laser ablation plumes are probed using multiphoton ionization time-of-flight mass spectroscopy. This is a versatile and sensitive technique of high mass resolution which can distinguish between compounds of similar masses and between isotopes. For certain important atomic isotopes, the superb spectral resolution of multistep resonant ionization, can detect minute (~100 attogram) samples and differentiate between a minor isotope buried in a 10^{10} fold excess of the naturally occurring isotope.

The advantages of the LAMS approach include: Small sample requirements, minimum sample preprocessing, minimum waste generation, and reliable technology. However, several uncertainties are introduced by the ablation process. For instance, it is not clear how well the composition of the ablated (gaseous) products reflects the sample composition; some sample components can be preferentially ablated. We have used several approaches to determine in more detail the mechanisms and consequences of laser ablation on model waste compounds and on relevant wide-band-gap inorganic materials. A detailed study of the ablation of a major waste tank constituent (sodium nitrate) has been completed. LAMS analysis of a variety waste tank constituents has also been performed and very encouraging results for the analysis of ethylenediaminetetraacetic acid and hydroxyethylenediaminetriacetic acid (EDTA and HEDTA both chelating agents) and waste simulant have been obtained. The technique of matrix assisted laser desorption ionization (MALDI), a variant of the LAMS technique, has been used to aid the analysis of the more complicated waste compounds. The MALDI technique involves adding a "matrix" compound to the waste sample to aid the laser vaporization and ionization process. Once vaporized, the analyte/matrix

plume contains both positive and negative ions which often provide complementary information.

For certain critical trace elements, it is also important to focus on the method of ionization of the ablated material. Technetium-99 has been identified as a significant ground water contaminant at a number of locations on the Hanford site. Because of its long half-life (214,000 years), high fission yield, and high rate of mobility in the subsurface, Tc-99 is considered a hazardous radioisotope waste. Furthermore, Tc-99 can be used as a critical path isotope for performance assessment of nuclear waste isolation barriers. Because Tc-99 is a long-lived pure beta-emitter, routinely available radiochemical-counting methods do not provide adequate sensitivity for use of Tc-99 as a performance assessment tool. However, the long half-life of Tc-99 does make it an ideal case for high-sensitivity detection by laser resonance ionization methods. Current efforts have designed optimal excitation schemes, using resonances that overlap the emission wavelengths of reliable diode and titanium-sapphire laser sources. Improvements on this methodology, are expected to ultimately result in a field-portable, routine analytical technology capable of rapid, accurate and sensitive measurements.

There are three major objectives of this research. First, to develop general and sensitive techniques for determining the molecular speciation of organics and inorganics in tank wastes and those chemisorbed on mineral soil substrates. Second, to develop new multiphoton-ionization schemes, based on reliable solid-state diode lasers, for detection of Tc-99 and other environmentally relevant atomic species. Third, to transfer this new knowledge to other applied DOE and DoD analytical programs such as the MARS and Hanford-site characterization programs. This report has been written in partial fulfillment of the third objective.

III. ACCOMPLISHMENTS

A. Waste Compound Analysis by Matrix Assisted Laser Desorption Ionization

We have recently used MALDI for the molecular analysis of a variety of known waste compounds. The MALDI technique works by embedding a low concentration of a high molecular weight (HMW) molecules in an excess of a carboxylic acid matrix. The matrix usually has a strong absorption resonant with the laser ablation wavelength such that the initial pulse energy is readily deposited into the matrix rather than into the analyte. The subsequent vaporization of the matrix produces isolated gas-phase biomolecules, often without significant fragmentation. The vaporized matrix provides another benefit

by enhancing the chemical ionization of the nascent gas phase species. When MALDI is combined with TOFMS one can measure an entire mass spectrum in a single analytical step requiring only a few microseconds. Since the MALDI process produces ions directly, very little material is required and thus MALDI is an efficient micro sampling technique that minimize radiation exposure for the analysis of highly radioactive samples.

Chelating compounds such as ethylenediaminetetracetic acid (EDTA) and N-(2-hydroxyethyl)ethylenediaminetriacetic acid (HEDTA), are receiving renewed analytical interest. Large quantities of EDTA and HEDTA (approximately 240 and 1500 tons, respectively) have been used in defense-related activities at the DOE Hanford site.[1] The chelators form water-soluble complexes with most heavy metals, thereby enhancing the migration of heavy metals in soils. For example, studies at Oak Ridge National Laboratory demonstrated that EDTA caused the low-level migration of ^{60}Co from intermediate-level liquid waste disposal pits and trenches.[2] Another study at the Maxey Flats commercial low level waste disposal site revealed that Pu-EDTA and ^{60}Co-EDTA migrated.[3] Analytical methods for chelators and organic acids, in radioactive wastes, generally involve derivatization and gas chromatography[4] coupled with mass spectrometry or liquid chromatography.[5] The MALDI technique has several advantages over other methods when applied to analysis of low molecular weight (LMW) compounds.[6] Due to the nature of the gentle ionization processes, chelators and other non-volatile species should remain intact during analysis without the need for time-consuming derivatization procedures.

We have used MALDI-TOF to examine anions, organic acids, and chelators. Samples of EDTA, HEDTA, citric acid, NTA and several of the inorganic anions including sulfate, phosphate, nitrate, and nitrite were analyzed, in high and low salt concentrations and over a wide pH range, to reflect conditions present in such wastes. Samples containing high salt concentrations can dramatically decrease MALDI sensitivity thus severely deteriorating analytical results.[7] In order to improve MALDI sensitivity for high salt content samples, we have processed some samples using cation exchange. In addition, we performed MALDI on mixtures of these compounds to simulate the combinations of compounds found in complex mixed wastes. All data were obtained using a linear TOF instrument with a nominal mass resolution of $m/\Delta m = 600$, positive and negative ion detection modes and a channeltron ion detector with an amplification of 10^5. An internal 337 nm nitrogen laser, of 3 ns pulse duration, is used to induce the desorption/ionization process.

We tried several standard matrix molecules (Fumaric, maleic, and succinic acids) and, as noted by other workers,[8] found 2,5 dihydroxy benzoic acid (DHB) to be the most efficient. In most cases, matrix molecules were mixed in water to a concentration of 10 mg/ml which is approximately a saturated solution. Analyte molecules were dissolved in water to the same concentration and combined, in various proportions, with the matrix solution. One (1.0) microliter of sample was applied to each spot on the sample tray. The MALDI spectrometer can be programmed to scan the laser beam focus across each individual sample spot. In all analyses, 100 evenly spaced laser pulses were collected and averaged per sample spot.

Since we are interested in determining the constituents of complex sample mixtures we performed MALDI on mixtures of several analytes including: oxalic acid, citric acid, ammonium sulfate, and ammonium nitrate. We parameterized the MALDI technique for analysis of LMW molecules by measuring the effects of varying the matrix to analyte molar ratio, the laser fluence, and the sample pH, on the analyte base peak ion signal. For most analyses, the matrix to analyte molar ratio was roughly 100:1. In one study, the ratio of matrix to analyte was varied systematically from 1000:1 to 0.1:1. The pH was varied for both citric acid and HEDTA analytes before the samples were applied to the sample tray. The pH values were adjusted using trifluoroacetic acid (0.1%), purified water, and 1% ammonium hydroxide to approximately 2, 5, and 10, respectively.

Figure 1 shows the positive ion MALDI spectrum of HEDTA and EDTA. The positive ion MALDI mass spectra of the chelators typically have strong base peaks indicative of the protonated $[M+H]^+$, and sodium adduct $[M+Na]^+$ peaks. The EDTA spectrum displays multiple sodium adducts $[M+nNa]^+$. At lower m/z strong ion signals attributable to the DHB matrix are observed; $[DHB-OH]^+$ at *m/z* 137, $[DHB+H]^+$ at 155, and $[DHB+Na]^+$ at 177.

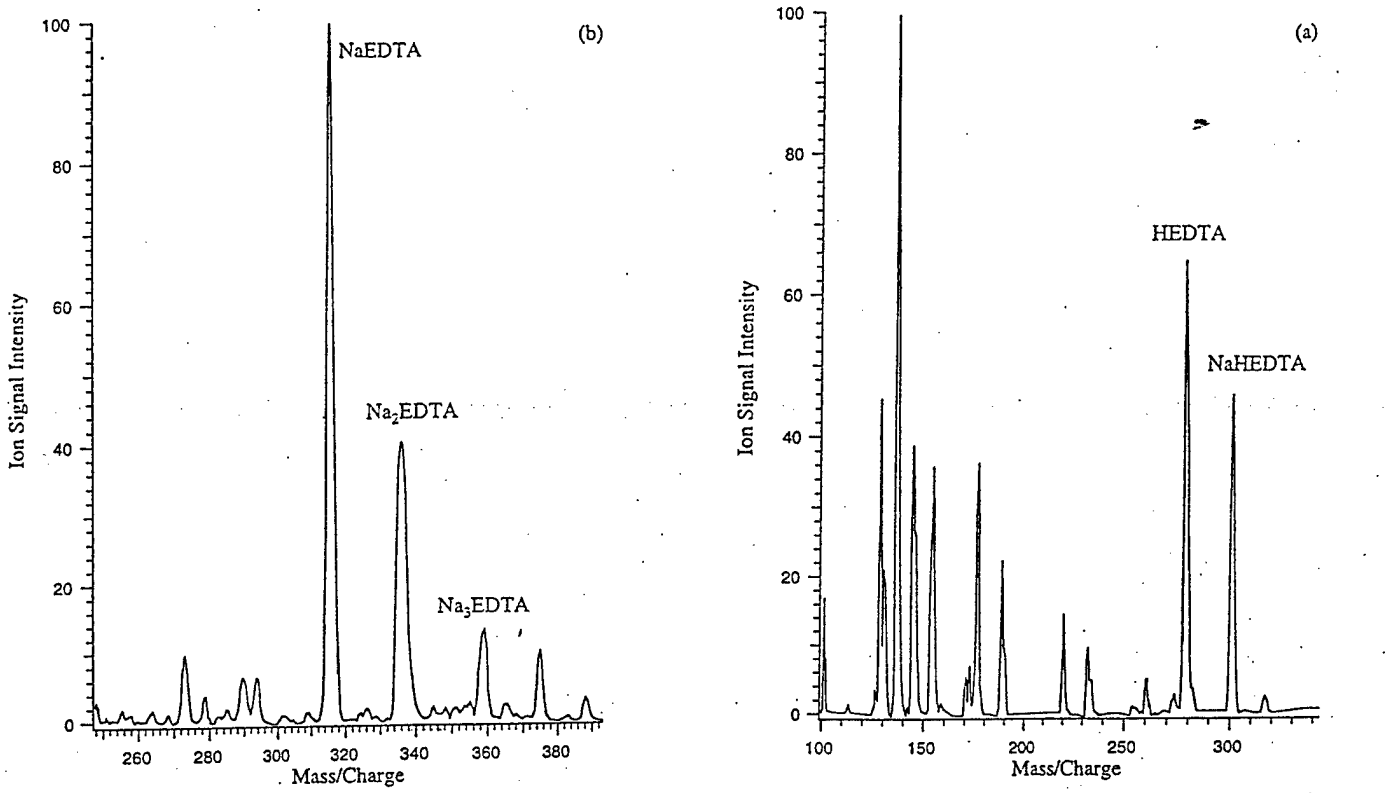

Figure 1. Positive ion MALDI spectra for (a) HEDTA and (b) EDTA in DHB at a matrix to analyte molar ratio of 100 to 1. The protonated $[M+H]^+$, and sodiated $[M+Na]^+$ are identified. Note the progression of sodiated peaks in (b) at m/z = 315, 337, and 359. The peaks at m/z= 137, 155, and 177 are attributed to ionized matrix species as described in the text.

Figure 2 shows the negative ion MALDI mass spectrum of citric acid, the strong negative ion signal is attributed to the deprotonated intact molecule $[M-H]^-$ at m/z=191. Figure 2 illustrates how little matrix interference can be present in the negative ion detection mode as only a single strong matrix peak is evident at m/z=153, $[DHB-H]^-$. The analytes studied and the m/z values and assignments of the ions observed in positive and negative ion MALDI-MS are shown in Table 1. Inspection of Table 1 reveals an interesting feature; the amine-based chelating compounds yield strong signals in the positive ion mode while the small organic acids and oxyanions yield strong signals in the negative ion mode. This effect is most easily rationalized on the basis of relative acidities and ion stabilities.

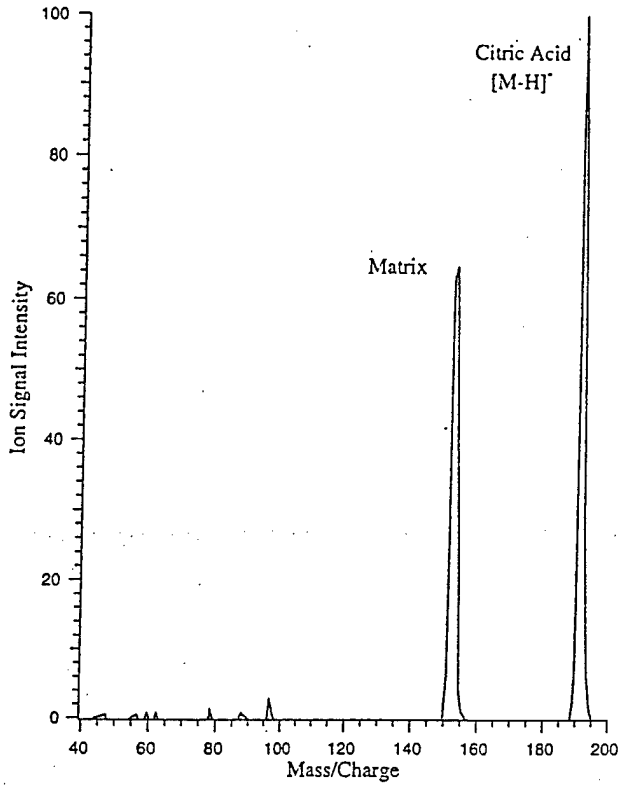

Figure 2. Negative ion MALDI mass spectrum for citric acid in DHB matrix at a matrix to analyte ratio of 100 to 1. The spectra displays only two significant peaks, the $[M-H]^-$ base peak at m/z=191 and the single matrix base peak $\{DHB-H]^-$ at m/z=153. The 'clean' mass spectrum and distinct lack of fragment or adduct peaks is characteristic of the negative ion MALDI of small molecules.

An important experimental consideration in MALDI analysis is the matrix:analyte molar ratio. For smaller molecules it has been suggested that a ratio of 100:1 to 1,000:1 is optimal.[6] This ratio contrasts with typical matrix:analyte ratios of 1,000 to 10,000 :1 for HMW species.[9] Figure 3 shows a graph of the base peak ion signal intensity versus the matrix to analyte molar ratio for the range 1000:1 to 0.1:1(negative ion mode).

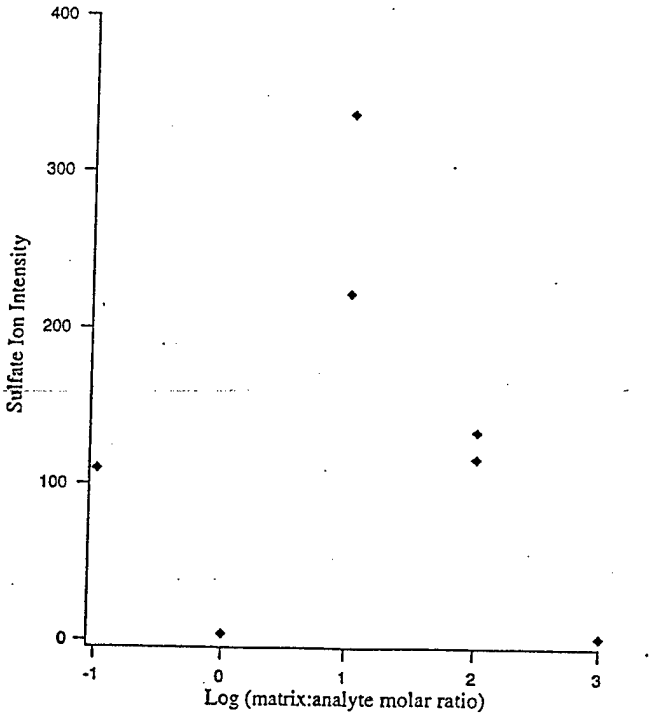

Figure 3. The integrated negative ion signal intensity versus the matrix to analyte molar ratio. The ion signal for citric acid $[M-H]^-$ in DHB matrix over the matrix:analyte molar ratio range of 1,000:1 to 0.1:1. Although strong signals are observed in the range 10:1 and 1:10, results were more consistent for the molar ratio of 100:1.

It appears from this figure that for sulfate ion a matrix:analyte molar ratio of 100:1 provides a good signal and our empirical observation is that the best signal to noise is obtained at this ratio. We note however that strong but less consistent signals are obtained at the lower matrix to analyte ratios of 10:1 and even at ratio's as low as 0.1:1. For certain waste analysis applications, such low ratio's may be useful. For example, the analysis of radioactive samples may not allow a full dissolution of contaminates in a waste stream. In this case, the application of a top layer of matrix material, followed by standard MALDI mass spectrometry could determine the adsorbed contaminant. Although the optimum matrix to analyte ratio differed for the various analytes, each analyte displayed a linear correlation similar to that of sulfate with increasing signal for increasing analyte fraction.

The range of suitable samples was further evaluated by changing the pH of the solution using trifluoroacetic acid and ammonium hydroxide. Figure 4 displays the base peak signal strength for samples containing citric acid and HEDTA prepared at three different pHs: 0.1% trifluoroacetic acid (pH ~2), Milli-Q water (pH ~5), and 1% ammonium hydroxide (pH ~10).

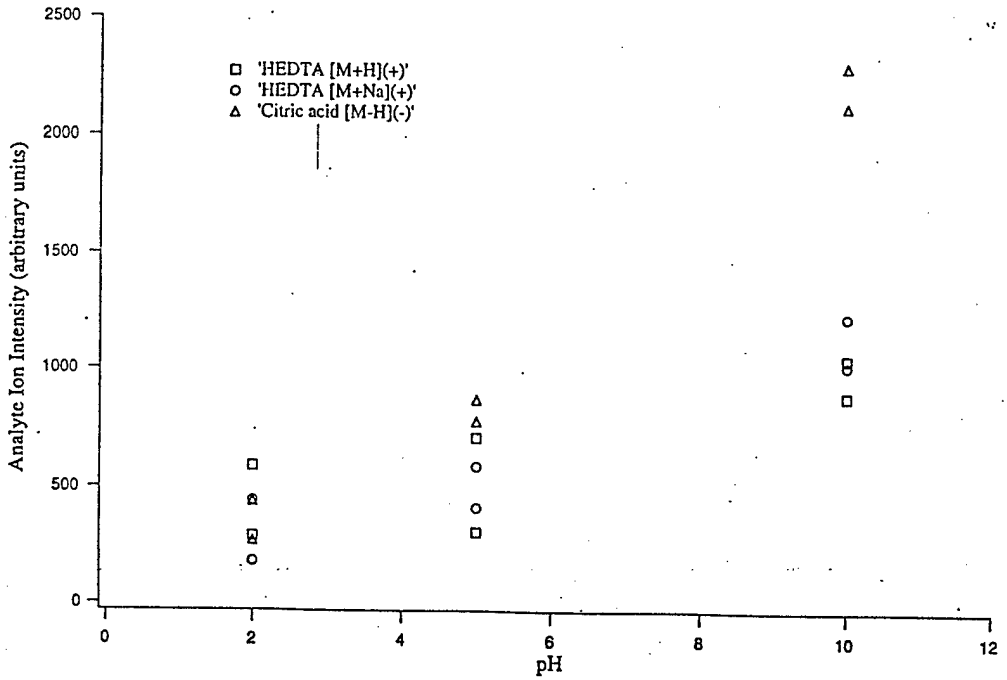

Figure 4. The influence of sample pH on integrate base peak intensity for citric acid and HEDTA analytes. The triangle symbols (Δ) designate citric acid in the negative ion mode $[M-H]^-$; the crosses (+) indicate the protonated HEDTA signal $[M+H]^+$; and the open circles (O) designate the signal from the HEDTA sodium adduct $[M+Na]^+$. All three base peaks increase monotonically with pH over the range pH=2 to pH=10.

All six samples were analyzed using both positive and negative ion detection modes. The strongest signal for all analyte ions was from samples of the highest pH regardless of detection mode polarity. The increase in base peak intensity with pH is most marked for the citric acid as the $(M-H)^-$ ion at *m/z* 191. The material contained in mixed waste storage tanks is often characterized by high pH so this result is an unexpected positive for our analysis efforts.

Hazardous waste is often a very complex mixture containing dozens of compounds. It was anticipated that, at the lowest matrix to analyte molar ratios, multiple analytes might interfere with one another, or that some analytes would preferentially associate with the matrix, resulting in poor sensitivity. Figure 5 shows the negative ion MALDI spectrum of a relatively equimolar mixture of citric acid, oxalic acid, ammonium sulfate, and sodium nitrate with DHB matrix (matrix to analyte ratio of ~1:4). All four analytes are readily observable although the nitrate ion signal at *m/z* =62 is considerably weaker than the three other analyte ion signals.

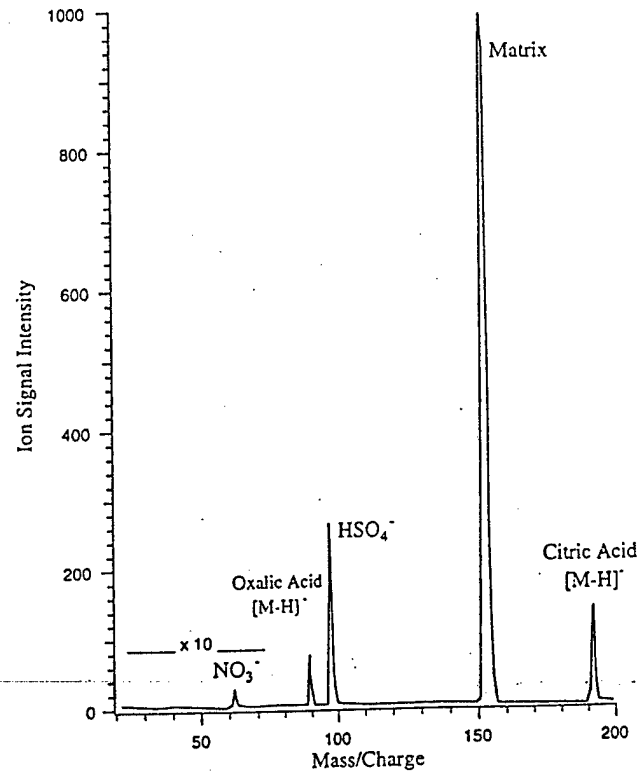

Figure 5. Negative ion MALDI spectrum of the analyte mixture consisting of equimolar concentrations of ammonium nitrate, oxalic acid, ammonium sulfate, citric acid and matrix (DHB). The matrix: analyte molar ratio is ~4:1. It is notable that all four analytes produce detectable signals although the intensity NO_3^- peak is significantly weaker than for the sulfate or organic acid analytes.

In an attempt to increase detection sensitivity in the analysis of samples containing or heavily contaminated with sodium or other alkali salts, we used an ion exchange resin to remove metal cations. Figure 6 displays the MALDI mass spectrum of sodium

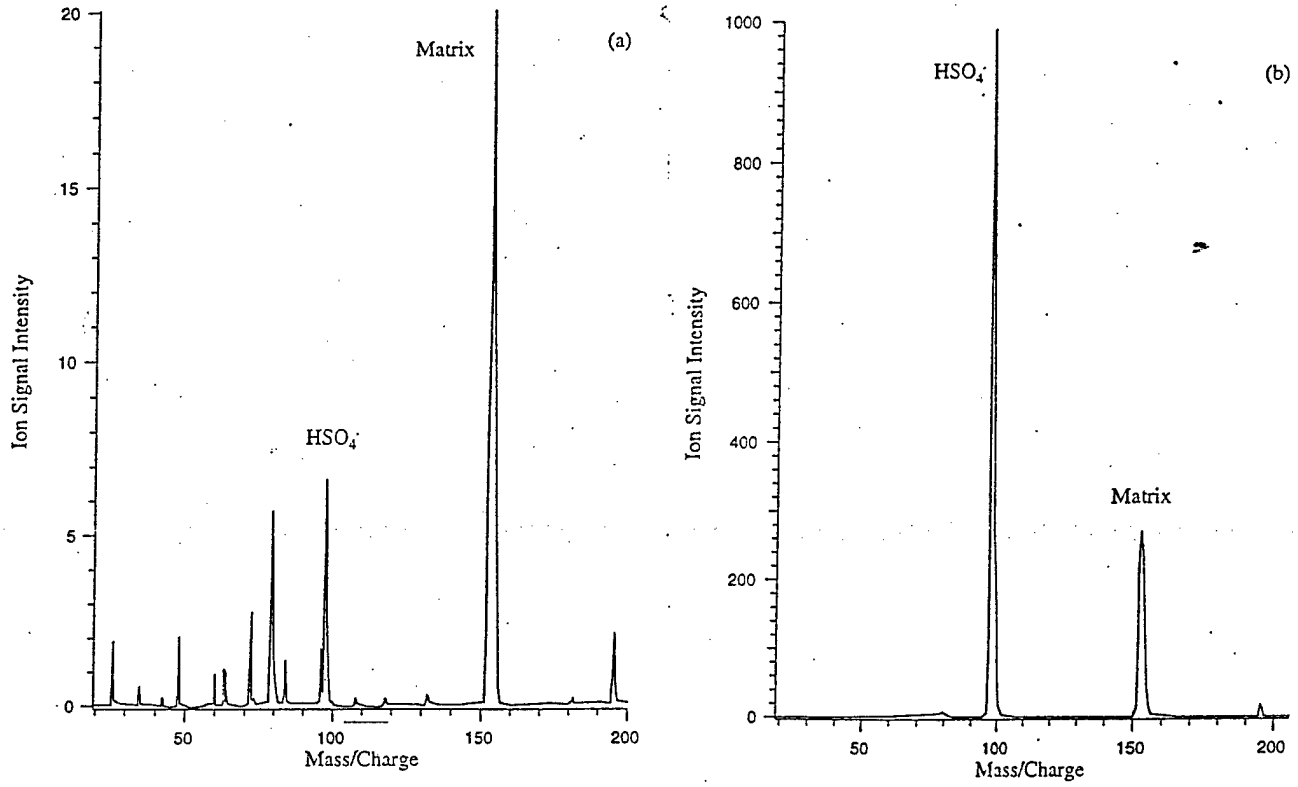

Figure 6. The negative ion MALDI spectrum of sodium sulfate before (a) and after (b) ion exchange. The HSO_4^- base peak increases by a factor of 140 while the matrix ion base peak increases by a factor of 15. Note the change in scale between (a) and (b). Sodium sulfate at a concentration of 10mg/ml was analyzed in DHB and compared with the MALDI signal produced after processing through an ammonium form ion exchange column (see text).

sulfate (before the ion exchange process) and ammonium sulfate after ion exchange. The absolute ion signal intensity of the HSO_4^- base peak increases by factor of 140. In addition the low mass "noise" is reduced with respect to the matrix ion signal at m/z = 137. The base peak intensity was typically one to two orders of magnitude larger following ion exchange for the same quantity of analyte material.

Low molecular weight but thermally non-labile species, while amenable to MALDI analysis, provide unique challenges and significant technical differences exist between low and high mass regimes. Many HMW biomolecules contain several acidic and basic functional groups. The amphoteric nature of the large molecules results in strong MALDI signals in both negative and positive ion channels. For smaller molecules either the positive or negative ion channel may be favored. Consider the detection of the organic acids listed in Table 1; these molecules are readily deprotonated forming stable anions. We may reasonably expect strong $[A-H]^-$ base peaks for organic acids. The results in Table 1 confirm this expectation. Similarly, the stable oxyanions NO_3^-, NO_2^-,

and HSO_4^- are readily observed in the negative ion channel. In studies of small proteins and peptides, Zhu et al. found that the positive ion signal of MALDI was strongly enhanced by the presence of basic amino acids in the chain. In that work, it was argued that a solution phase pre-proton transfer mechanism is responsible for the enhanced positive ion signals.[10] Similarly, our target chelating compounds EDTA, HEDTA, and EDDA are amine derivatives (i.e. good bases) which form stable adducts with H^+ and Na^+ leading to strong base peak signals in the positive ion channel.

Table 1. Positive and Negative ions observed by MALDI-TOF MS

Analyte	Molecular Weight	Ions Observed (m/z)	
		(-)	(+)
Sodium Nitrate	85	62 $[NO_3]^-$	
Sodium Nitrite	69	46 $[NO_2]^-$	
Oxalic Acid	90	89 $[M-H]^-$	
Fumaric Acid	116	115 $[M-H]^-$	
Maleic Acid	116	115 $[M-H]^-$	
Succinic Acid	118	117 $[M-H]^-$	
Ammonium Sulfate		132	97 $[HSO_4]^-$
Citric Acid	192	191 $[M-H]^-$	
IDA	134		157 $[M+Na]^+$ 173 $[M+K]^+$
HEDTA	278		279 $[M+H]^+$ 201 $[M+Na]^+$
EDDA	176		177 $[M+H]^+$ 199 $[M+Na]^+$
NTA	191		192 $[M+H]^+$ 199 $[M+Na]^+$
EDTA	292		293 $[M+H]^+$ 315 $[M+Na]^+$ 337 $[M+2Na]^+$ 359 $[M+3Na]^+$

Sodium ion adduction is often observed in MALDI, even for samples that do not contain sodium.[11] In these cases, the sodium impurity is introduced through minor contamination of the matrix material. Sodium adduction competes efficiently with proton adduction at low levels of contamination. For samples containing a significant sodium component, such as Na_4EDTA, we expect and observe a strong $[EDTA + Na]^+$ peak. We also observe the adduct series $[EDTA + nNa]^+$, n=1-4. Although multiple adduction of sodium is rare[11] such species may reasonably be expected for a tetra-dentate chelator such as EDTA. The series of peaks at m/z=315, 337, and 359 form a very characteristic pattern which strongly over determines the data set needed for detection of EDTA in solid samples. This is significant in that prior attempts at detection of chelators have proven quite difficult as the techniques of laser desorption ionization

(LDI), and secondary ion mass spectrometry (SIMS) produce severely fragmented mass spectra. [12]

Figure 6 displays the relationship between MALDI sensitivity and sodium contamination. A possible mechanism for the reduced analyte ion yield involves the stealing of charge by both neutral (Na^o) and ionized (Na^+) sodium atoms. The ionization potential of isolated sodium neutral is 5.1 eV significantly lower that of either the matrix or the analyte. An excess of Na^o in the desorption matrix or plume could react or exchange charge with positively charged matrix or analyte, thus neutralizing analyte molecules and their ionization source. Since Na^o requires only ~ 5 eV to ionize, we may expect significant Na^+ concentrations in the desorbed plume. Collisions of Na^+ in the matrix of plume with negatively charged analyte molecules will rapidly neutralize these species as well. Hence, high sodium concentrations appear capable of simultaneously degrading both positive and negative ion yields. There are a variety of other plausible mechanisms for signal degradation by sodium salts.

In our efforts to apply MALDI to the analysis of high sodium content samples we removed sodium by cation exchange. The exchange of NH_4^+ for Na^+ yielded a sensitivity increase of a factor of roughly 100. It is anticipated that by using this ion exchange process a wide variety of small molecules contained in high salt content mixtures, can be easily analyzed by MALDI-TOF MS. Similarly the simultaneous detection of combinations of analytes is promising for obtaining semi-quantitative analysis of more complex mixtures. Future efforts will be directed at advancing quantitative aspects of waste analysis measurements because, at present, ion signals are often erratic. Progress toward quantitative analysis of HMW species has occurred only recently for well characterized samples. [6, 13-18] The difficulties encountered in attempts to obtain quantitative yields are due to the many factors which determine MALDI efficiency such as matrix/analyte effects, laser wavelength and power, morphological effects in sample crystallization, [19, 20] and the complex nature of the MALDI technique. As yet, most of the operative mechanisms involved in MALDI are poorly understood. [11, 21-25] Nonetheless, recent progress using internal standards, [6, 13, 17, 18, 26] data analysis techniques, [16] and co-matrices[14] is encouraging and we expect that, with more work, MALDI will become a reliable quantitative technique for solid waste analysis.

Initial experiments on infrared matrix-assisted laser desorption/ionization mass spectrometry (IR-MALDI) using a free electron laser in the analysis were completed. Mass spectra from samples of ethylenediaminetetraacetic acid (EDTA), nitrilotriacetic

acid (NTA) and a phosphate salt were obtained. Low molecular weight (LMW) compounds are of similar mass as the molecular weight of the matrix compound and interference between matrix and analyte ions can degrade MALDI sensitivity. Under optimal conditions, however, we found little interference and that often the analyte signal exceeded the matrix signal, a result also observed in UV-MALDI of these compounds. In the IR MALDI of EDTA near 3.0 μm the FEL results are similar to those obtained using a fixed frequency 2.94 μm Er:YAG laser of 200 ns pulse duration. However, the tunable FEL laser can selectively excite particular vibrational modes of the matrix (e.g. an OH or CO stretch) or of residual water contained within the crystalline MALDI sample.

Infrared MALDI

In general, MALDI is regarded as a qualitative rather than quantitative analytical technique. Greater understanding of the complex mechanisms involved in both UV and IR MALDI is needed to make quantitative analysis possible. We have completed initial IR MALDI studies of EDTA in succinic acid, a matrix which has been extensively studied using free-electron, Er:YAG and CO2 lasers. [27] We find that the IR MALDI irradiance threshold is a strong function of sample morphology. Moreover, the wavelength dependence of the MALDI threshold does not simply track the absorption of either the succinic acid matrix or the EDTA analyte.

The experimental details are reported in an upcoming publication. [28] Briefly, the Vanderbilt FEL was tuned over the range 2.8-6.5 μm delivering pulse energies from 20 to 60 mJ in a 4 μs macropulse. The IR optical train incorporates a fast electro-optic switch (Pockels cell) to slice a short micropulse train ($t \geq 100$ ns) out of the nominal 4 μs FEL macropulse. [29] Each macropulse comprises about 10^4 micropulses 1 ps in duration, separated by intervals of 350 ps. The spatial pulse structure is a clean TEM_{00} mode. A $f =$ 85 mm lens focuses the beam, producing a spot on the target measuring approximately 300 μm in diameter. The mass spectrometer is a linear time-of-flight mass spectrometer equipped with a microchannel plate detector. It consists of a one-meter TOF tube and a turbomolecular-pumped vacuum chamber with a base pressure of 10^{-8} torr. The analog ion signal from the microchannel-plate detector is ac-coupled to a 10x pre-amplifier and digitized by a LeCroy 9310M transient recorder at time intervals of 10 ns.

The samples were prepared in accordance with the standard "dried-droplet" protocol. The succinic acid matrix was dissolved in water to a concentration of 30 mg/ml, to

produce a nearly saturated solution. Analyte molecules Na_2EDTA and EDTA -free acid were dissolved in water to concentrations of 5 mg/ml and 0.5 mg/ml respectively. The matrix and analyte solutions were combined in matrix:analyte ratios ranging from 10:1 to 300:1 on the stainless steel substrate. A 10 microliter sample drop was applied to the substrate and dried for 10 minutes in a stream of unheated air. Sample crystal structure was observed using an optical microscope prior to introduction of the dried sample into the vacuum chamber.

Figure 7 displays the TOF mass spectra for 2.94 μm MALDI of EDTA following excitation from an Er:YAG laser and the Vanderbilt FEL. The MALDI response, from a succinic acid matrix, is quite similar for the long pulse (200 ns) of the Er:YAG and the 100 ns pulse train of the FEL. Although the 100 ns portion of the macro pulse provides a similar irradiance as the YAG pulse the fluence of each micro pulse is 1000 times greater. That the MALDI threshold depends upon irradiance rather than fluence is contrary to UV MALDI results[30] as noted in recent FEL MALDI work. [27]

Figure 7(a)

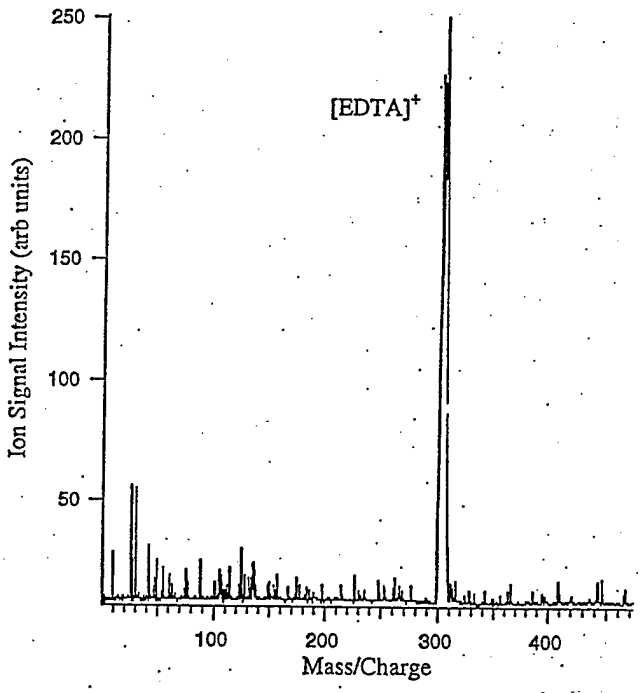

Figure 7(b)

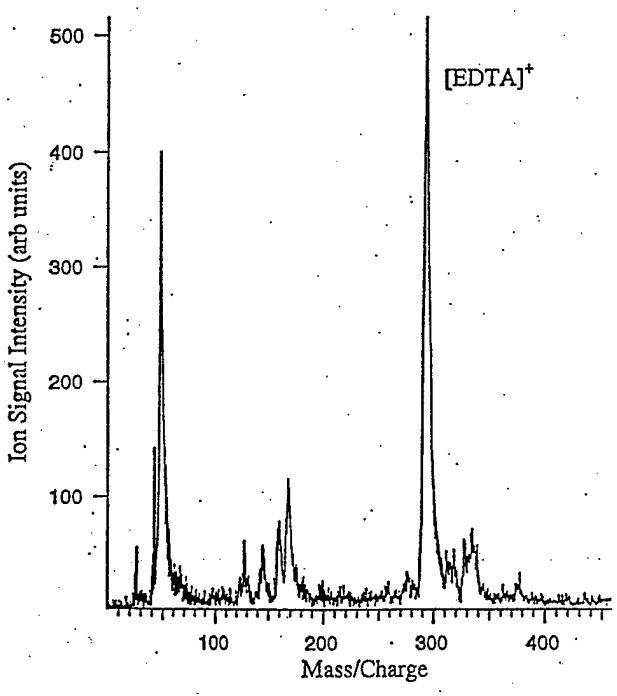

7) Comparison of FEL (a) and Er:YAG spectra (b) of EDTA at 2.94 μm. The FEL IR MALDI spectra display a strong parent mass peak and little matrix ionization. Considerable variability are observed on a shot-to shot basis however, and we conclude that FEL and Er:YAG MALDI at 2.94 μm produce largely similar mass spectra. The mass shift observed between the two spectra is an artifact of the linear TOF mass spectrometer and is likely due to different initial velocities of the analyte ions.

We observe no ions without added matrix molecules as the EDTA laser desorption ionization threshold is higher than the MALDI threshold. Near threshold both analyte and matrix ion production is low; on the order of a few hundred ions. The 100 ns switched out FEL pulse has a similar number of micropulses. Thus, if ion production is evenly distributed throughout the switched out pulse then each micropulse generates only a small number of ions. However, it is possible that the early micropulses excite the matrix and this excitation is prerequisite for more extensive ion generation by later pulses. This later scenario is consistent with the observation that the duration of the ion pulse generated by the 100 ns switched-out pulse is itself less than 100 ns. [27] At this time, FEL pulse length studies are limited by the Pockel's cell technology which produces an 80 ns minimum pulse duration.

Figure 8 displays the TOF mass spectra for UV MALDI of EDTA in a 2, 5-dihydroxy benzoic acid matrix obtained using the same experimental apparatus. In this case, a 337 nm nitrogen laser, of 3 ns pulse duration, is used to induce the desorption/ionization process. The output of the nitrogen laser is focused to a rectangular spot 200 μm x 100 μm at the sample.

Figure 8(a)

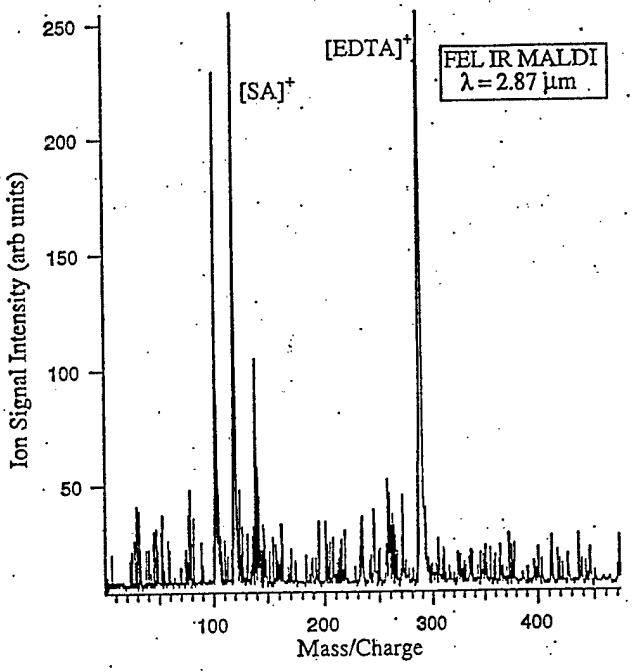

Figure 8(b)

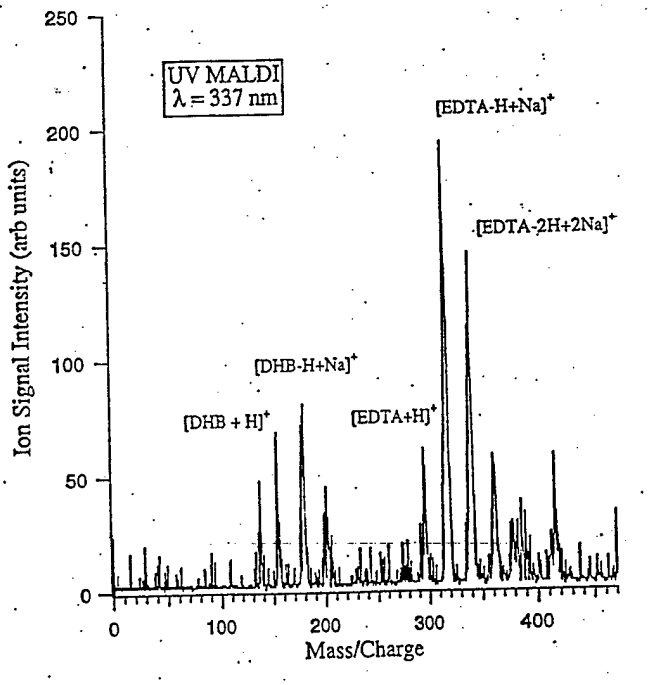

8) Comparison of single-shot FEL MALDI spectra (2.87 μm) and UV MALDI (337 nm) spectra of EDTA in succinic acid. The UV MALDI mass spectrum displays greater matrix ionization and sodium adduction than does the IR MALDI mass spectrum. We note that the ion signal intensity and "quality" are similar in each mass spectrum.

The TOF spectrum displays strong protonated, $[M+H]^+$ and sodium-adducted $[M+Na]^+$ peaks; where M represents the free acid EDTA. The EDTA spectrum also displays $[M-H+2Na]^+$ and $[M-2H+3Na]^+$. At lower m/z strong ion signals attributable to the DHB matrix are observed; $[DHB+H-H2O]^+$ at m/z =137, $[DHB+H]^+$ at m/z = 155, and $[DHB+Na]^+$ at m/z = 177. The series of sodium adduct peaks forms a highly characteristic pattern. Specific differences between the UV and IR results includes the increased relative strength of the $[M+H]^+$ and $[M-2H+3Na]^+$ peaks. This pattern of a pronounced series of sodium adducts extends further than the sodium adduction observed in the IR MALDI. A second difference between IR and UV MALDI is the strong readily identifiable matrix ion peaks apparent in the UV MALDI TOF. The IR MALDI spectra often display only analyte ion peaks (for a succinic acid matrix at least). Furthermore, when matrix associated ions are observed, the masses observed are greater than the molecular weight of the matrix. This may indicate that reaction of the matrix is occurring prior to matrix ionization. The clean mass spectra obtained in IR MALDI may be associated with this additional complexity in the matrix ionization mechanism.

The MALDI response obtained in the 5 to 6 μm region displays a distinct wavelength threshold near 5.9 μm. At wavelength of 5.9 μm and greater, few analyte ions are observed. However, for wavelengths between 5.4 and 5.8 μm analyte ions are readily observed. Oddly, the wavelength threshold does not correlate directly with IR absorption bands of either the succinic acid matrix or the Na_2EDTA analyte. One might expect the absorption threshold to decrease linearly or superlinearly, with sample absorption as a function of wavelength. The IR absorption spectrum of the matrix displays a strong C=O stretch band centered 5.9 μm. The short wavelength tail begins near 5.6 μm and extends to 5.0 μm. Therefore it is surprising that the MALDI threshold is obtained only for wavelengths less than the 5.9 μm absorption maximum. A similar threshold wavelength behavior has been observed previously in the IR MALDI of small proteins in the 3 μm (OH stretch band) and 6 μm (C=O stretch band) regions. [27] In both the current and previous studies, the MALDI threshold is higher for wavelengths near the band center than for wavelengths well into the "blue edge" of the absorption band. A plausible explanation for this behavior assumes that surface species, whose absorption maxima are shifted to higher frequencies, yield analyte ions much more easily than bulk species. The question remains as to whether the absorption bands are shifted enough to mirror the threshold wavelength dependence. Other plausible mechanisms have been discussed recently. [27]

The relative threshold irradiance for an analytically useful MALDI response has been qualitatively determined in two wavelength regions. The O-H and C=O stretching bands of succinic acid centered at 3.3 and 5.9 μm, respectively, provide strong IR absorption and are excellent targets for FEL MALDI. Figure 9 displays the succinic acid absorption spectrum and relative MALDI threshold in the 2.5 to 6.5 μm region. The usual model for UV and IR MALDI assumes that a strong matrix absorption feature must have considerable overlap with the emission wavelength of the excitation source. Therefore, one might expect that the MALDI threshold, as a function of wavelength, will mirror the target absorption feature. We find that, contrary to these expectations, the lowest MALDI threshold, for excitation of the O-H stretch band, is at 2.87 μm and, for the C=O stretch band, near 5.7 μm. Both threshold minimum are well off the peak of the IR absorption features.

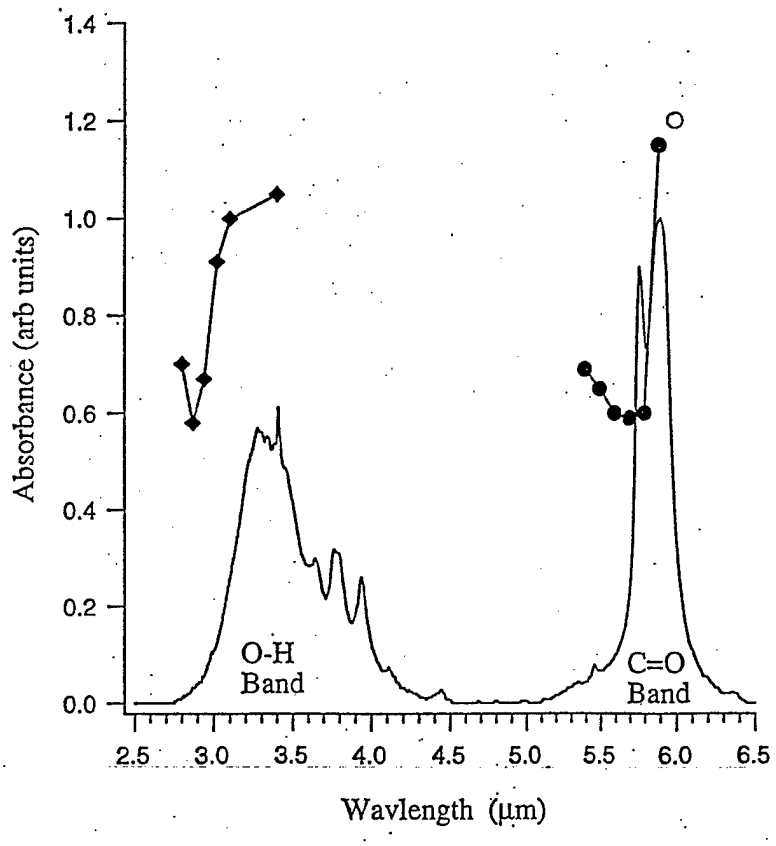

9) Relative threshold for IR MALDI of EDTA in succinic acid in the 6 μm (solid circles) and 3 μm (solid diamonds) regions. The minima in MALDI threshold is shifted to the high energy side of the C=O and O-H stretch band maxima. The open circle indicates that no MALDI response is observed at 6 μm and greater wavelengths.

We must add a considerable cautionary note when discussing MALDI threshold determinations. The erratic nature of both UV and IR MALDI signals has been noted throughout the literature. While the cause of the large fluctuations in MALDI ion production is due to several factors, including the highly nonlinear power dependence, inconsistent sample preparation is a strongly suspected source of signal fluctuation. Since sample preparation involves rapid crystallization (usually) and crystallization is quite sensitive to sample concentrations and environmental conditions, multiple crystal structures can be observed for even similar preparation procedures. During the course of these experiments we noted at least two different regimes of crystal growth. The dominant growth regime produced large icicle-like or rock-like crystals while the minor growth regime produced much finer dendritic crystals. The different crystal structures, in turn, yielded quite different irradiance thresholds for the MALDI response.

The desorption and ionization mechanisms in IR-MALDI has been much debated. One possibility in the present case is that MALDI is due to thermal desorption. The temperature rise of the substrate during a single 100-nm FEL pulse (sliced out from the macropulse by the Pockels cell) is approximately[31]

$$\Delta T \approx \frac{F(1-r)}{\rho C_p \mu} \leq \frac{0.5\ J \cdot cm^{-2} \cdot 0.05}{7.9\ g \cdot cm^{-3} \cdot 0.5\ J \cdot g^{-1} K^{-1} \cdot 1.1 \cdot 10^{-4} cm} \approx 60\ K \qquad (1)$$

where the reflectivity $r \approx 0.95$ in this wavelength range; the fluence F is typically 0.5 J·cm^{-2}; the heat capacity at constant pressure is C_p; and the thermal diffusion length is

$$\mu = \sqrt{D \cdot \tau_{laser}} \equiv \sqrt{\left(\frac{\kappa}{\rho C_p}\right)\tau_{laser}}$$
$$= \sqrt{\left(\frac{0.5\ W \cdot cm^{-1} K^{-1}}{7.9\ g \cdot cm^{-2} \cdot 0.5\ J \cdot g^{-1} K^{-1}}\right)\ cm^2 \cdot s^{-1} \cdot 10^{-7}\ s} = 1.1 \cdot 10^{-4}\ cm \qquad (2)$$

The value for ΔT is substantially less than the (460 K) melting or vaporization temperature of the succinic acid (about 300K). This is in fact an overestimate of the temperature rise in the substrate, since the reflection, absorption and scattering losses in the MALDI sample are neglected. We therefore conclude that the substrate-heating effects on the MALDI process are negligible, as previously noted by the Hillenkamp group. [30]

In the other extreme case of assuming that all the energy is absorbed by the matrix material (at λ = 2.94 μm) the temperature rise in the MALDI sample is calculated to be[32]

$$\Delta T \approx \frac{\alpha F(1-r)}{\rho C_p} \leq \frac{250\ cm^{-1} \cdot 0.5\ J \cdot cm^{-2} \cdot 1}{1.57\ g \cdot cm^{-3} \cdot 1.3\ J \cdot g^{-1} K^{-1}} \approx 60\ K \qquad (3)$$

where it is assumed that the reflectivity $r \approx 0$; $\alpha = 250\ cm^{-1}$ is the optical absorption coefficient for succinic acid at λ = 2.94 μm. The difference between the Eqns. 2 and 3 arises from the fact that in case of the stainless steel substrate the optical absorption depth is relatively short but the thermal conduction is quite large and has to be taken into account, in case of succinic acid matrix material, on the other hand, the optical absorption depth is quite large whereas the thermal conduction is negligibly small. Even if the absorption of the laser energy occurs partly in the matrix material and partly in the substrate, the overall temperature rise in the MALDI sample will be around 60 K. This temperature rise is substantially less than that required to induce melting or vaporization of the matrix material and supports spallation as a possible mechanism for MALDI process.

A substantial MALDI response is present even for wavelengths that do not overlap the main absorption feature and are better described as overlapping the short wavelength tail. These results clearly contradict IR MALDI models that assume the threshold fluence is proportional to the energy deposited in a finite sample volume. The measured threshold wavelength dependence is, however, consistent with the findings of Cramer et al. in an FEL MALDI study of a variety of aliphatic and aromatic matrices.[27] In that work a model based on spallation, and the concomitant creation of charged species during the bond-breaking process, was suggested. Such a model is consistent with spallation coupled to surface desorption and ionization.

B. Laser Ablation Mass Spectrometry

A modified ultrahigh vacuum (UHV) mass spectrometer has been used to characterize individual waste compounds and waste simulant using the LAMS technique. Using this apparatus, the optimal laser-ionization frequency and pulse duration has been determined for detection of selected molecular species in the UV region between 50,000 and 37,600 wavenumbers (cm^{-1}). In particular, specific ionization schemes for desorbed species NO and CO have been determined. Laser pulse durations of 10 ns, 5 ns and 60 ps have been investigated for nitrate waste compounds. Excellent speciation of waste compounds EDTA, HEDTA, and succinic acid has been obtained using matrix assisted laser desorption ionization and additional studies building on these successes are in

progress. To explore the details of laser ablation we conducted an in-depth LAMS study of sodium nitrate; a major Hanford-site tank waste component.

Sodium nitrate is a by-product of the chemical processes used to extract plutonium and as such constitutes a large fraction of Hanford-site tank waste. Over 150,000 tons of sodium nitrate are believed to be contained in the radioactive tank and crib waste and analysis of such wastes must account for the effects of this compound on the analysis technique. [10] From the standpoint of molecular chemical analysis, solid $NaNO_3$ is an excellent test of the LAMS method: Although the molecular formula is simple, yielding straightforward mass spectrometric analysis, the electronic and crystal structures are complex and complicated dynamics are likely during laser ablation. Indeed, the molecular speciation of salts such as sodium nitrate has proved difficult for LAMS and other analytical techniques. This is due, in part, to the ionic nature of the material which leads to facile plasma formation and the subsequent reactions of molecular species present in the ablation plume. For these and other reasons, we selected sodium nitrate for a detailed investigation by LAMS and other analysis techniques.

We have used several approaches to explore the various dynamical regimes of UV ablation of sodium nitrate. Important experimental parameters including laser wavelength, power, and pulse duration for both the ablation and the ionization lasers were systematically investigated. The ablation laser wavelength was tuned from near 266 nm to 193 nm covering a region in which the material optical properties range from nearly transparent to very strongly absorbing[33] Different ablation mechanisms were found to dominate for resonant versus non-resonant laser ablation. The relative importance of each mechanism was also found to depend upon the condition of the sodium nitrate sample. For example, resonant ablation of a pristine sample of crystalline sodium nitrate produces molecular fragments at much higher yields than does longer wavelength nonresonant ablation. However, after exposing the sample to high radiation fluxes or electron bombardment, to simulate radiation damage as would be found in real waste samples, equally high yields can be obtained for either resonant or nonresonant ablation. The increased ablation yield of radiation damaged samples is likely due to defect-mediated mechanisms. [34] To understand the resonant ablation mechanisms, we performed ab initio calculations on crystalline sodium nitrate, and isolated NO_3, NO_2^-, and NO_3^-. The results of these calculations reveal the details of the laser ablation mechanism for resonant excitation of crystalline sodium nitrate. [3]

Resonant Laser Ablation

We have completed an investigation of the laser desorption of NO from single crystal sodium nitrate following pulsed 213-nm excitation of the $\pi^* \leftarrow \pi$ absorption band localized on the nitrate anion. The excitation laser flux was maintained at low levels (< 2 MW/cm^2) to obtain product distributions free of secondary interactions following fragment ejection from the crystal surface. Neutral NO is the predominant desorption product although a smaller yield of neutral O_2, much less than the stoichiometric ratio, is also observed. No significant desorption of NO_2 or Na is detected under low laser fluence. [35] At low fluence, no plasma is formed and the NO photodesorption yield is found to be linear with desorption laser power indicating that single photoabsorption events lead to fragment ejection. The desorption yield is enhanced by roughly a factor of 1000 for resonant excitation (213-nm) over nonresonant excitation (266-nm) on a per-photon basis. We determined the relative vibrational, rotational, and translational energy distributions of the neutral NO photoproducts to be 1.0:0.4:0.3:0.3:0.2 for the v=0:1:2:3:4 levels indicating significant vibrational excitation of the product NO. The vibrational product state distribution indicates that NO desorption is the final step of a photochemical process (exciton decay) that results from decomposition of NO_3^{-*} on or near the crystal surface. [35] The rotational state populations and translational energy distributions are well characterized by thermal distributions at the substrate temperature of 293K. The dissociation mechanism differs from that reported for dissociation of gas phase ions due to the stabilization of the ions by the crystalline field. The role of bulk exciton migration is unclear at present however, an ongoing effort to measure the desorption quantum yield may address this issue. We are currently investigating the contribution of defect absorption and exciton migration, to the overall reaction mechanism, by measuring the wavelength dependence of the $\pi^* \leftarrow \pi$ absorption band, and by laser polarization studies which exploit the birefringence of the sodium nitrate crystal.

Nonresonant Laser Ablation

For nonresonant laser ablation higher fluences are required for observable molecular emission. The principle neutral product observed by exposing single crystal sodium nitrate to 248-nm excimer laser radiation is still NO (at fluences of approximately $80mJ/cm^2$ as measured using a quadrupole mass spectrometer). The intensity and identity of the ablated products however, are a strong function of the laser fluence and previous sample exposure. [36] In particular, a strong incubation effect is observed, with weak emission intensities during the early stages of irradiation which grow

dramatically with continued irradiation. Figure 10 displays a sigmoid shaped emission versus laser exposure curve that characterizes the incubation behavior. From this data, it is apparent that defects created by NO emission, on more or less perfect $NaNO_3$ surface, strongly enhance subsequent emission. The strong enhancement of NO emission due to prior laser damage indicate that, under these conditions, emission is largely defect-mediated. At higher laser fluences (>100mJ/cm^2 on laser-incubated surfaces), other neutral products, primarily O_2 and Na, are emitted along with NO. at fluences near 80mJ/cm^2 on heavily irradiated surfaces, only weak O_2 emission is observed.

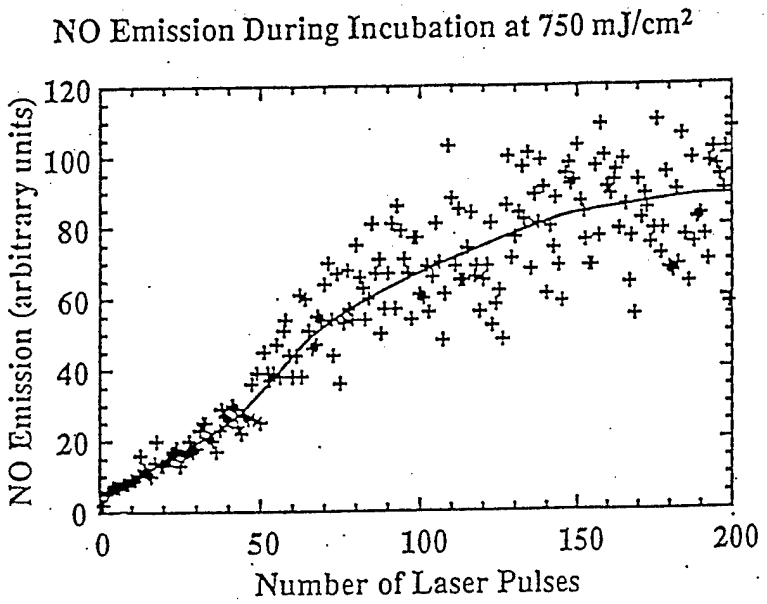

10) Incubation behavior of crystalline sodium nitrate irradiated with repeated 248 nm excimer laser pulses. Repeated laser pulses induce increasing neutral NO emission by inducing defects in the sodium nitrate crystal. The laser fluence is 750 mJ/cm^2 per pulse.

Figure 11 displays the mass spectra produced under increasing laser pulse energy. Above 80mJ/cm^2 the NO emission intensity rises sharply along with increasing O_2 and Na emissions; weaker emission at heavier masses are also observed. At these higher fluences, laser induced heating and nonlinear laser-plasma interactions (etching) further enhance the emission intensities resulting in a strong nonlinear dependence on laser fluence.

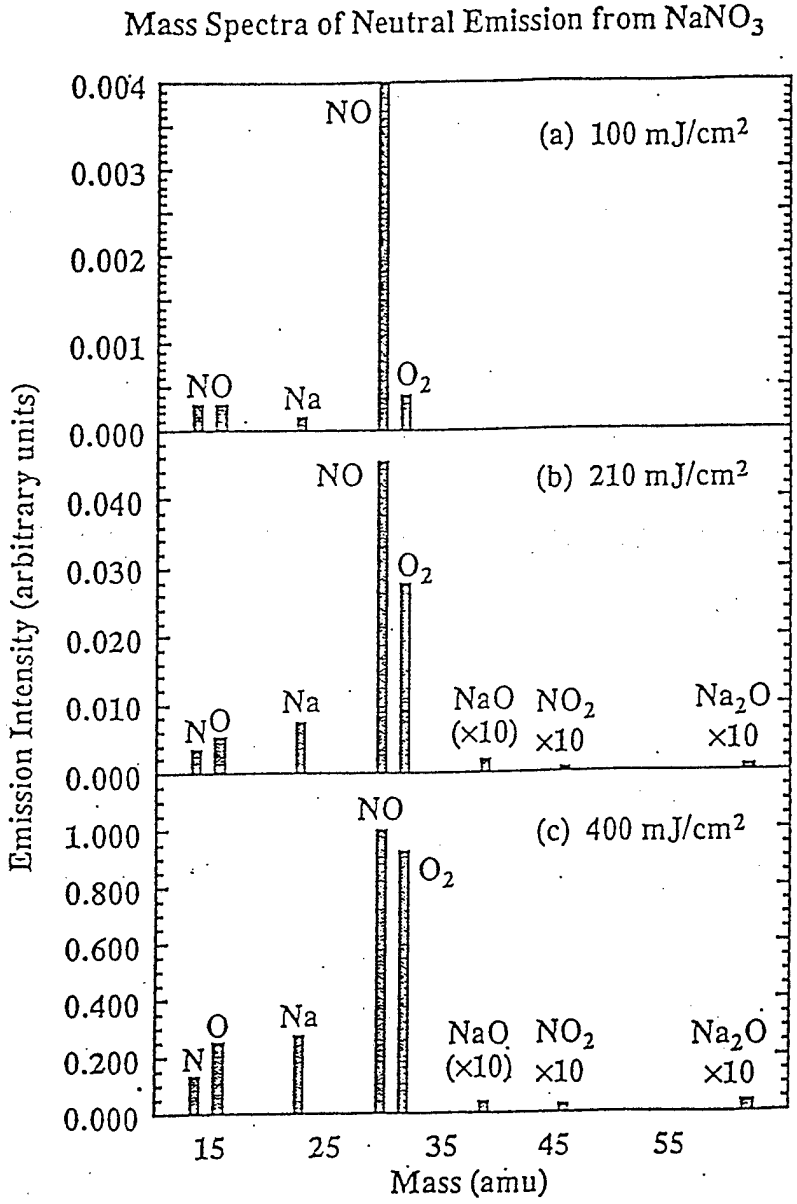

11) Mass spectra of 248 nm laser induced emission from $NaNO_3$ irradiated at fluences of (a) 100 mJ/cm², (b) 210 mJ/cm², (c) 400 mJ/cm² per pulse.

The neutral emissions produced by 248-nm radiation share much in common with the neutral emission accompanying bombardment with 1-3 keV electrons. [34] Both processes yield similar products with similar product velocity distributions. Not surprisingly, defects created by electron irradiation significantly enhance subsequent laser-induced emissions and lower the fluence required for plasma formation. Similar effects have been also observed in other radiological sensitive, wide bandgap materials. We further note that alkali nitrate matrices containing radioactive impurities (such as Hanford-site tank waste) will contain high densities of similar defects which will strongly affect LAMS-based analytical techniques.

Theoretical Studies

We have used ab initio quantum mechanical methods to calculate the electronic properties of the bulk material, and the clean and defected surfaces of crystalline $NaNO_3$. The results of these calculations provide insight into the photoexcitation/desorption mechanism and support the conclusions drawn from the experimental investigation. Ab initio periodic Hartree-Fock (PHF) calculations indicate that the electronic structure of bulk $NaNO_3$ and the clean cleaved crystal surface are nearly identical, indicating that the absorption profile of the bulk and surface nitrate anions will be the same. Hence, for laser desorption on an undefected sample the photo absorption cross-section is the same for surface and bulk chromophores. This result is consistent with the experimental observation that the NO photodesorption yield (from the clean surface) mimics the bulk absorption profile (i.e. minimal sub-bandgap desorption is observed).[3] Changes in the excitation spectra are, however, expected to occur when the surface is chemically or structurally defected. Converting NO_3^- to NO_2^- groups on the surface is energetically facile and could possibly occur during experimental sample preparation or irradiation.[37] The presence of surface NO_2^- groups is predicted to cause a shift in electron density into the gap region, producing a +1 eV to +2 eV red shift in the surface absorption profile. Such a red shift is inferred in the LAMS experiments from the high NO yield induced by sub-band-gap irradiation energies, for heavily defected surfaces. The molecular-ionic nature of this crystal is evident from the band structure (calculated using PHF). The cationic (sodium) and anionic (nitrate) valence bands are well-separated and flat across the Brillouin zone, with a large gap between the top of the valence and the bottom of the conduction bands. Nitrogen and oxygen orbitals combine to form the "molecular-like" nitrate bands. The uppermost valence bands in the bulk and clean surface are derived predominantly from oxygen 2p orbitals. Photoexcitation of the $\pi^* \leftarrow \pi$ transition is from these states to the lowest unoccupied states, which are formed from an equal mixture of oxygen and nitrogen 2p orbitals.

The "localization" of the 6 eV band on the nitrate ion is due to the "molecular-like" character of crystalline $NaNO_3$. The assignment of this band to the $\pi^* \leftarrow \pi$ transition is based on the spectroscopy of other nitrate compounds (in solids and in solution).[33, 38] The "molecular-like" spectroscopic properties of this material have been probed by quantum mechanical CASSCF calculations of the ground and excited state energies of the gas phase species (NO_2^-, NO_3^-, and NO_3). These high-level ab initio calculations on

the isolated gas-phase species reaffirmed the spectroscopic assignment based on earlier molecular orbital calculations[39, 40] The effect of the crystalline environment on the transition energies was investigated by embedding NO_3^-, NO_2^- and NO_3 in a finite array of charges mimicking the first two nearest-neighbor shells in the bulk. All of the states (ground and excited) of the negative ions (NO_3^- and NO_2^-) were equally stabilized by the electrostatic field; thus the transition energies did not change when the ion was placed in the mock crystal field. [3] In contrast to the negative ions, no stabilization of neutral NO_3 occurred when it was embedded in the point charge array. The lack of significant stabilization causes the neutral photodetachment channel to be inaccessible in the 6 eV photoexcitation of the crystal such that the direct dissociation of exited state nitrate $(NO_3^-)^*$ to form NO + O_2^- is the energetically allowed pathway. The NO is then ejected from the crystal, leaving O_2^- trapped (for some time) on the surface. Since the yield of O_2 to NO yield is far less than stoichiometric, the resonant desorption experiments are consistent with the O_2^- trapping mechanism.

Several conclusion may be drawn from the laser ablation studies of sodium nitrate. It is clear that while it is possible to understand the detailed mechanism involved in NO emission from a pristine sodium nitrate crystal, the emission process itself changes the composition of the crystal surface and therefore the emission mechanism. Any accurate analysis technique based on the NO yield must therefore take into account the condition and exposure history of the sample. Furthermore, the condition of the "matrix" of waste molecules constituting the solid sample can dramatically affect the composition of the ablation plume. Following the detailed studies of solid sodium nitrate we began a series of experiments on other known waste compounds singularly and in combination with sodium nitrate. In the latter case, $NaNO_3$ may be considered the matrix for laser ablation. Figure 12 displays the mass spectra obtained following laser ablation of Na_3PO_4 embedded in an excess of sodium nitrate. The dominant peak is atomic phosphor with less intense features at the PO, PO_2, PO_3, and PO_4 masses. The ablation wavelength (213 nm) is efficiently absorbed by both the nitrate and phosphate chromophores leading to fragmentation of these species. Similar results are obtained for the analogous sulfate salts. It is also apparent that LAMS of phosphate and sulfate salts produce highly fragmented mass spectra and only weak parent ion signals. This is in sharp contrast to the strong parent molecular ions observed in MALDI mass spectrometry of these oxyanions. It is clear that sodium nitrate is not a "good matrix" material and that use of far UV wavelength leads to fragmentation.

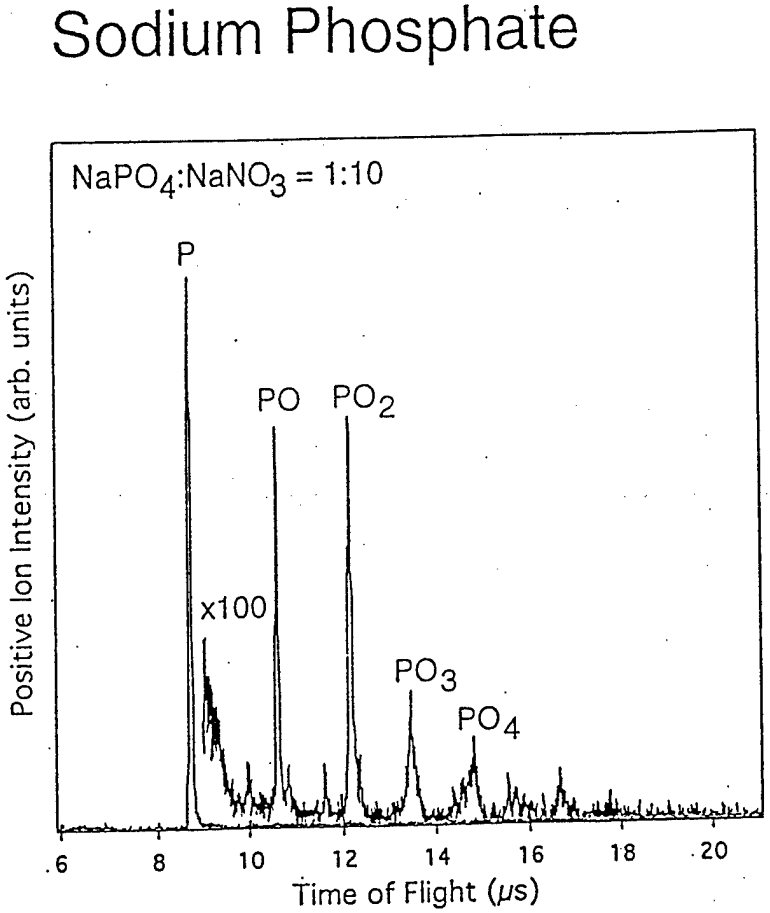

12) Laser ablation mass spectra phosphate salts. While only a weak parent mass peak is observed, the fragmentation pattern itself is characteristic of the presence of phosphate.

Femtosecond Laser Ablation

Environmental samples are often difficult to analyze for possible contamination, requiring sophisticated analytical techniques such as matrix-assisted laser desorption/ionization (MALDI) and laser ablation mass spectrometry (LAMS). Generally, nanosecond lasers have been used as the irradiation source for laser ablation, however many of the key processes (i.e. electron/hole-pair recombination, trapping, electron/phonon interactions, etc.) involved in laser/solid interactions occur on a sub-nanosecond time-scale. An important first step in optimizing methods based on laser ablation lies in the understanding of these fundamental processes. The goal of this portion of our research effort is to study these important aspects involved in energetic laser/solid interactions, where the solid material is usually an environmentally relevant wide-band gap material, such as magnesium oxide, calcium carbonate or sodium nitrate.

Femtosecond transient absorption spectroscopy is one of the most widely used techniques in the study of ultrafast dynamics in transparent materials. In a typical transient absorption experiment, a subpicosecond pump pulse excites carriers (electrons and holes) in a material, the absorption of a second subpicosecond probe pulse is measured as a function of delay between the pulses. The wavelength of the probe pulse is selected such that it is absorbed by the transient carriers, therefore the temporal evolution of the transient absorption can be related directly to the carrier dynamics (e.g. recombination or trapping, etc.). Transient absorption spectroscopy measures the change in the *imaginary* part of the index of refraction resulting from pump pulse excitation.

Recently, the addition of a frequency-domain interferometric detection technique to a traditional pump/probe transient absorption apparatus has increased the amount of information that can be obtained in a time-resolved experiment. [41-43] Namely, the transient phase shift of the probe pulse, as well as any transient absorption, can be obtained. The transient phase shift of the probe pulse is a measure of the change in the *real* part of the materials index of refraction upon pump pulse excitation. Information about both the real and imaginary parts of the index of refraction forms a complete picture of the materials dielectric response (i.e. charge-carrier dynamics) to the excitation pulse.

Obtaining the transient phase shift is accomplished by measuring the shift of the spectral interference pattern between a reference pulse and the probe pulse which arrive at the sample before and after the pump pulse, respectively. Figure 13 is a schematic representation of our experimental optical arrangement for transient phase measurements, the inset depicts the relative timing of the reference, pump and probe pulses. The reference and probe pulses are identical and are generated in a simple Mach-Zehnder interferometer in which a temporal delay between the pulses can be set.

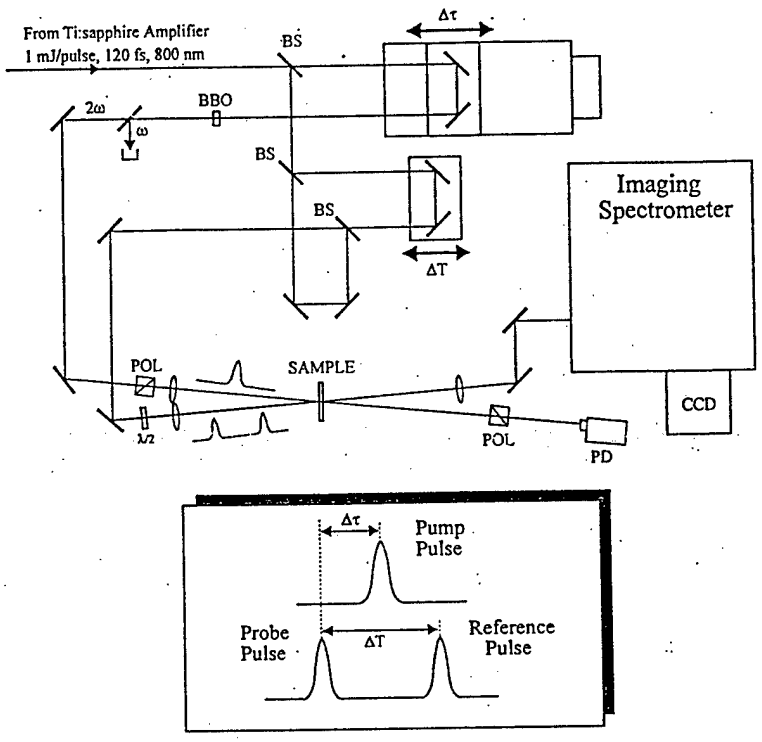

13) Experimental optical layout for transient phase measurements. The crossed polarizers and the half-wave plate in the pump and reference/probe beams respectively, allow for a 3rd order cross-correlation Kerr signal to be detected in the pump beam, simplifying spatial and temporal overlap of the beams in the sample. The inset shows the relevant timing between the reference and probe (ΔT) and pump and probe beams (Δτ).

A periodic intensity modulation (with a spacing, $\Delta\omega$) is observed in the spectral profile of the reference/probe pulse-pair, and is related to the temporal separation (ΔT) of the reference and probe pulses via, $\Delta\omega=2\pi/\Delta T$. Examples of such interference spectra with different values of ΔT are shown in Figure 14 (in the absence of any pump pulse).

The probe pulse will experience a different index of refraction, from the reference pulse, if the pump pulse has excited a sufficient number of charge-carriers in the material, thereby causing an induced phase shift in the measured spectral profile of the pulse-pair. A decrease in the spectral modulation depth is observed if there is an accompanying transient absorption of the probe pulse. By measuring the magnitude of the phase shift and any absorption as a function of temporal delay between the pump and probe pulses the real and imaginary parts of the index of refraction can be inferred and used to describe the dielectric response of the material as a result of the pump pulse excitation.

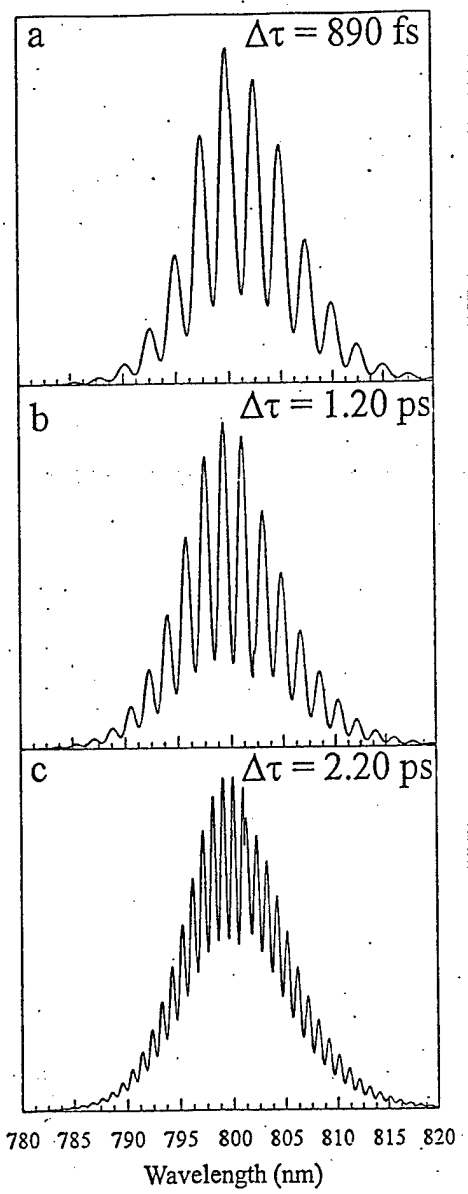

14) Frequency interference spectra of the reference/probe pulse-pairs shown with various amounts of temporal delay ($\Delta\tau$). The decrease in fringe contrast with increasing delay is attributed to the finite spectral resolution of the spectrometer.

A mode-locked Ti:sapphire oscillator, producing < 100 fs pulse widths at a repetition rate of 82 MHz, is used to seed a Ti:sapphire regenerative amplifier (pumped at 20 Hz by the frequency doubled output of a Q-switched Nd:YAG laser) which increases the energy of the femtosecond pulses into the 1-10 mJ/pulse range while maintaining pulse widths ~ 120 fs. The system is capable of producing energy densities > 10^{15} W/cm^2. The fundamental wavelength of the system can be tuned from ~750-850 nm, while

frequency doubling and tripling in nonlinear crystals can be used to extend the wavelength coverage into the visible and UV. Plans are underway to extend the wavelength into the VUV and soft X-ray region using high-harmonic generation in rare gases. Using the techniques described above we hope to gain additional insight into some of the key energetic processes which accompany laser/solid interactions. Of particular interest in these materials, is the role which defects may play in effecting the deposition of laser energy.

We have studied pulsed UV laser ablation of Ca^+ from the calcite form of $CaCO_3$. Calcium ion emission is observed following non-resonant excitation using the 3 ns Nd:YAG fourth harmonic, at 266 nm, and the 500 fs, 264 nm, and frequency tripled output of an amplified titanium sapphire laser. The absorption of ultra-intense femtosecond pulses can occur through different mechanisms than for nanosecond pulses. High power femtosecond pulses are often absorbed by nonlinear multiphoton excitation. This is in contrast to the sequential *multiple* photon processes characteristic of nanosecond laser excitation. Since the ultrafast absorption mechanism operates in a regime dominated by collisional and multiphoton ionization, the energy is absorbed by the electrons much faster than it is transferred to the lattice. This leads to a sharpening of the ablation threshold (in dielectrics at least) because there are no statistical fluctuations in the number of starting electrons, as is the usual case for nanosecond pulsed excitation. The distinct physical processes, which come into play on the ultrafast time scale, provide interesting new routes for material ablation. Our preliminary study of the non-resonant laser ablation of calcium carbonate illustrates the importance of the laser pulse duration. Figure 15 displays a comparison of nanosecond versus femtosecond laser desorption. Following nanosecond pulsed excitation (266 nm, 3 ns Nd:YAG) we find two distinct features in the emitted Ca^+ velocity distribution. The early arrival time feature contains only high velocity Ca^+ (with translational energies up to 100 eV) while the longer time feature is due to plasma plume likely containing Ca^+ and possibly other ions. When 500 fs laser pulses are used, only the early time feature is generated. The clear implications are that the early time feature results from a multiphoton material response while the longer time feature results from a sequential *multiple photon* mechanism. These results are in sharp contrast to resonant 157 and 193 nm excimer laser excitation of calcite. Resonant nanosecond excitation leads to predominantly neutral CO emission at much lower irradiances (< 1 MW/cm^2). In this low pulse energy regime, the neutral desorption yields were measured and the translational, rotational and vibrational degrees of freedom were characterized.

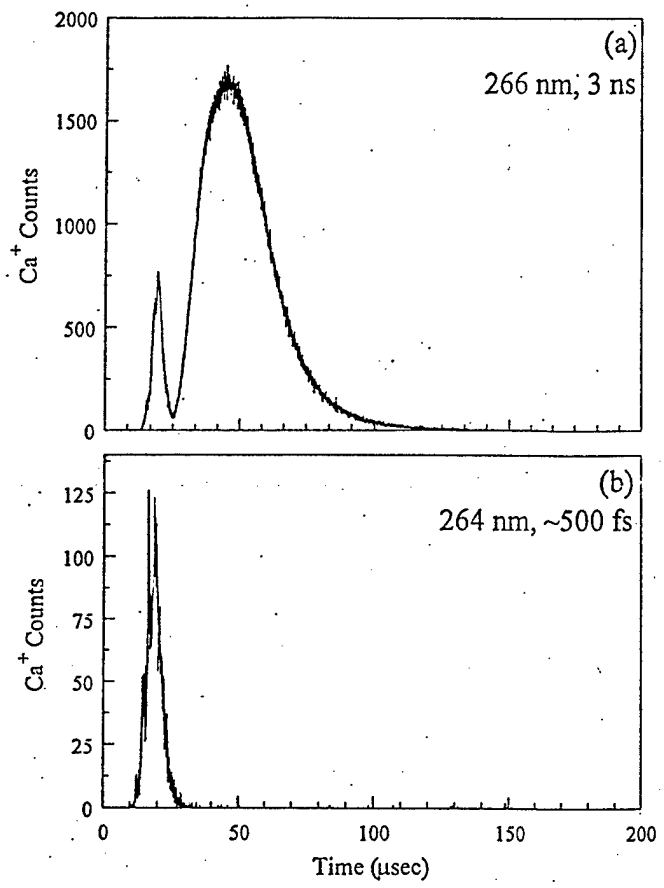

15) Time of flight spectra for Ca^+ desorbed from cleaved calcite following nanosecond and femtosecond excitation. The 3 ns, 266 nm pulse from the frequency quadrupled Nd:YAG produces two distinct features (a). The early-time feature is due to fast calcium ions while the broad late-time feature is not mass discriminable by the quadrupole mass spectrometer. The ~500 fs, 264 nm pulse from the frequency tripled Ti:sapphire amplifier produces only the early-time feature (b). In the case of the ultrafast excitation, (b), there is no possibility of laser plume interactions.

C. Development of Diode-Laser-Based Excitation Schemes for CW Resonance Ionization of Technitium

Solid state diode laser technology has undergone rapid development in recent years due to their immense commercial impact. As a consequence of this development, device reliability, power, wavelength range and tunability have improved dramatically. Diode lasers are now frequently used in atomic and molecular spectroscopic applications. [44] The emission characteristics of room temperature diode lasers, although often suitable for such spectroscopic applications, can in general be improved from the "naked" diode laser configuration by using an external cavity to provide selective feedback. We have developed one of the simpler selective feedback configurations, the Littrow grating cavity, as a reliable and optimized source for analytical spectroscopy applications. The

following results were obtained using a sharp LTO-015 diode laser nominally operating at 834 nm: Any desired wavelength in the region 818-848 nm can be reached by coarse tuning of the grating angle and minor (<1%) adjustments of injection current. Linewidth < 3 MHz (probably <1 MHz but current measurements are limited by available interferometer resolution) have been achieved without observable (>0.05%) side modes. Continuous, single-frequency tuning of 8-10 GHz is possible using piezoelectric scanning of the external cavity length. Output power up to 12 mW is readily obtained, however, for longevity and stability, typical output power is limited to 8 mW. It should be noted that continuous scanning regions greater than the observed 8-10 GHz can be achieved either by synchronously scanning injection current with external cavity length or by using specially prepared diode lasers with antireflection coated output facets.

Optimal Laser Ionization Schemes

A large number of three-step laser excitation schemes for selective ionization of technetium have been investigated at the University of Mainz. However, all of those methods have used only the wavelengths that are generated by copper-vapor-laser pumped dye lasers. Unfortunately, the lowest lying allowed transitions are in the violet and ultra-violet regions of the spectrum and thus it was necessary to frequency-double for the first step. In all cases, the excitation was from the $4d^55s^2\ ^6S_{5/2}$ ground state to various components of the $4d^65p$ configuration between 313 and 318 nm. While this is in the best range for the available frequency-doubled dye laser wavelengths, it is not optimal in terms of atomic spectroscopy since it involves relatively weak intercombination (two-electron excitation) transitions. The second step excitations were generally of a one-electron nature, for the most part into various fine structure components of the $4d^66s\ \{^6D_J\}$ configuration using wavelengths between 787 and 821 nm. The final ionization step then used excitation to various unassigned autoionizing levels using wavelengths between 650 and 850 nm.

It should be possible to improve considerably on the excitation schemes described above using the output of frequency doubled diode lasers. Several general principles have been used to select a more optimal excitation scheme. These include: 1) Only allowed, one-electron transitions should be used. 2) Choose $\Delta J = \Delta L = +1$ for all transitions in order to maximize transition probabilities. 3) If possible, ladder excitation should begin with the bluest (most energetic) photon and progress to lower energy photons in the subsequent steps, because increased laser power is generally required to saturate the subsequent steps. Allowed transitions out of the ground state can usually be saturated with approximately 1 mW laser power (1 mm diameter beam) while

saturation of excitation to Rydberg states requires several hundred milliwatts. Limiting the intensity of energetic photons in this manner minimizes background from nonresonant multiphoton processes. 4) The final step should involve photoionization of a Rydberg state atom using a continuous wave (CW) carbon dioxide laser. This is actually an extension of (3) and prior work at PNNL has shown that this can lead to CW saturation of the ionization step, even in the absence of autoionizing resonances, without significant production of background. These criteria lead directly to the schemes detailed in Figure 16. In the case of technitium, the excitation steps are: $4d^5 5s^2$ $^6S_{5/2}$ (ground state) 429.82 nm to $4d^5 5s5p$ $^6P_{7/2}$ (23265.33 cm^{-1}), 461.81 nm to $4d^5 5s5d$ $^6D_{9/2}$ (44919.07 cm^{-1}), 741 - 764 nm to $4d^5 5snf$ $^6F_{11/2}$ (58000 - 58400 cm^{-1}, n = 14 to 20) and 10.6 μm ionization step. It is worthwhile to note, particularly for routine analytical measurements, that the three resonance steps may be performed with diode lasers. The first two steps require frequency doubling of the diode lasers into the blue region of the optical spectrum.

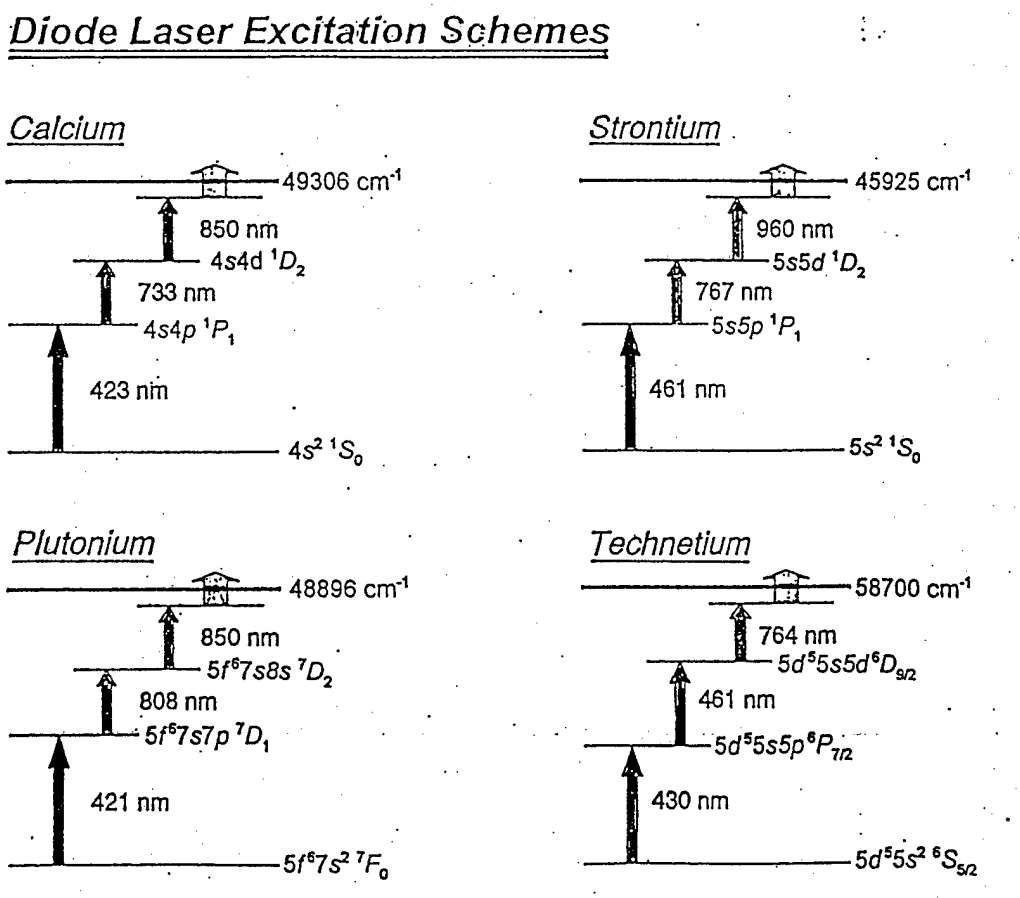

16) Schematic of optimized cw laser ionization schemes for technitium, strontium, plutonium, and calcium.

Frequency doubling the external cavity diode laser

Extending the operation of diode lasers into the blue region is essential for a wider range of applications. Only a limited number of elements, including heavier alkali metals, some lanthanides, and actinides have strong resonance transitions that are accessible to the normal red and near infrared operating regions of diode lasers. Many more elements have strong transitions in the spectral region which could be covered by frequency doubled diode lasers. Of particular interest here are the resonance lines of technetium and strontium at 428 and 461 nm, respectively. These wavelengths can be reached with the relatively inexpensive and relatively powerful diodes operating between 840 and 925 nm and using potassium niobate as the frequency doubling medium. Fortunately, potassium niobate has very high nonlinear coefficients and can be non critically phase matched for these wavelengths by temperature tuning. Both are important for obtaining efficient doubling of lasers with only tens of milliwatts of continuous power in the fundamental beam.

The efficient frequency doubling of diode lasers has been achieved and is a major accomplishment of our SERDP effort. A CW diode laser operating at 846 nm with an output power of 7 mW has been frequency doubled to a blue wavelength of 423 nm using a temperature tuned potassium niobate crystal in an external ring enhancement cavity. Figure 17 displays the schematic design of the external ring cavity. With the design used, frequency doubling efficiencies of approximately 15% are reached routinely and reliably.

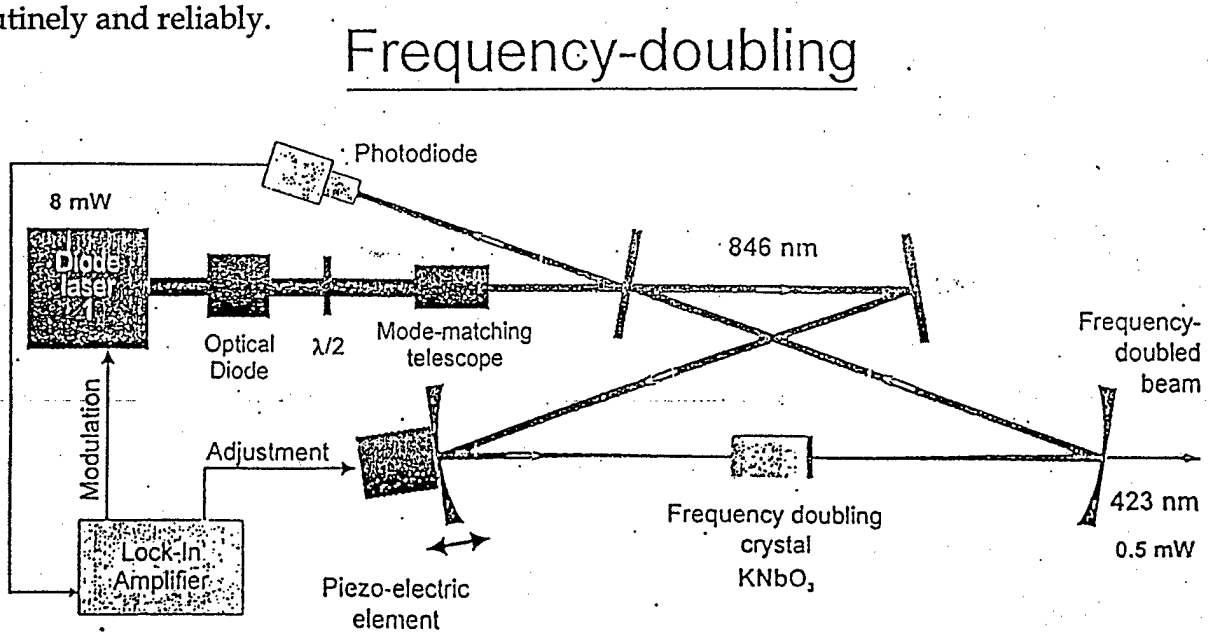

17) Schematic design of the external ring cavity used for efficient frequency doubling of ~840 nm room temperature diode laser. Doubling efficiencies of 15% are routinely achieved.

After losses from Brewster windows and ring output coupler mirror, usable 423 nm power is typically 700 microwatts. This power is generally sufficient to saturate Doppler-free allowed atomic resonance transitions that are used as the first step in multiple-resonance RIMS studies.

However, with available, more powerful diode lasers it should be easily possible to scale the frequency doubled output powers into the 10 mW range, if needed. With available diode lasers and the temperature tuning range of potassium niobate it is possible to generate wavelengths between 415 and 470 nm. Species of interest relevant to nuclear waste problems that can be addressed by these wavelengths include Tc-99 (430 nm), Sr-90 (461 nm), Cs-135,137 (455 nm), Plutonium (421 nm), and Uranium (426) nm.

Locking to Atomic Reference Signals

Stabilizing the frequency of high resolution CW lasers is necessary for reliable analytical measurements. For reproducible measurements the frequency must be held constant to within a small fraction of the natural atomic linewidth over periods of several hours. The frequency of the external cavity diode laser has been locked to an atomic reference signal. Three different types of measurements were used and evaluated for locking the laser frequency. These included normal absorption, saturated absorption, and optogalvanic spectroscopy. In all cases, the detected signal (photodiode detection of transmitted laser intensity for absorption measurements, and change in hollow cathode discharge impedance for optogalvanic measurements) was analyzed with a lock-in amplifier, which produces a derivative signal suitable for feedback and driving the laser frequency to the center of the absorption line. All three approaches were found to provide suitable results: It was possible to lock the laser to the atomic line center for periods up to 60 hours (2 days typical) when working with the diode laser fundamental frequency, demonstrating the type of long term stability that is mandatory for routine analytical measurements. In similar experiments, the above described frequency doubled diode laser has been locked to the Doppler free resonance line of Ca-40 in a small (2-3/4" conflat cross) atomic beam apparatus. Residual frequency modulation of ~2 MHz, which results from locking of the doubling ring cavity, is detected in absorption by the atomic beam with a lock-in amplifier. This results in a derivative signal suitable for feedback to the laser frequency control, holding the laser frequency on the center of the atomic absorption. This method has successfully locked the laser frequency to the atomic transition for periods of up to eight hours, limited by long term thermal drift of the ring doubling cavity. It is expected that with the use of temperature

thermal drift of the ring doubling cavity. It is expected that with the use of temperature stabilization or improved materials that stable frequency locking, of several days duration, can be achieved.

Frequency Shifting

Frequency locking to an atomic absorption can be performed realistically only for high abundance, naturally occurring isotopes, as is the case for Ca-40. Then, measurement of rare isotopes requires shifting of the laser frequency corresponding to the optical isotope shifts. For isotope shifts up to ~1 GHz this can be done easily and reliably with acousto-optic modulators. We have demonstrated frequency shifting of the doubled diode laser over the range of 135-175 MHz (appropriate to the measurement of the long-lived radioisotope Ca-41) with 85% efficiency in the first order Bragg diffraction. The remaining undiffracted (zeroth order), which is not frequency shifted, is then used for locking to the reference atomic absorption. This method provides a relatively simple and absolute frequency locking scheme. However, there are cases where no stable reference isotopes are available, e.g., technetium and plutonium. Here, fringe offset locking techniques with a Zeemann stabilized He:Ne laser, as has been previously developed and used at PNNL, can be used to achieve comparable laser frequency stabilization.

The development of optimal laser ionization schemes followed by the technological advances of external cavity control, ring cavity frequency doubling, and locking and shifting of the diode laser output, provide the necessary technical tools for routine utrasensitive detection of technetium, strontium, and other elements. The reliability of solid state diode lasers makes them the tool of choice for such analysis. These results indicate that an applied engineering effort to design and build an ultrasensitive analytical apparatus, that is based on solid state diode lasers, is worth strong consideration.

IV. CONCLUSIONS

The Laser Ablation/Ionization Characterization of Solids Program has succeeded in achieving many goals including the molecular speciation of a variety of known waste compounds and combinations of compounds and the development of excitation schemes and diode laser technology for ultrasensitive detection of radioisotopes. The early laser ablation studies characterized the important processes for analysis of high salt content waste and exposed the limitations of the LAMS technique for certain classes

of waste samples. This knowledge, in turn, led to the exploration of matrix assisted laser desorption ionization and the speciation of important waste compounds and combinations of waste compounds. The results of the MALDI studies are extremely encouraging and indicate that an entire class of chelating agents, their degradation products, organic acids, and several oxyanions are amenable to rapid molecular analysis.

We have recently refocussed the direction of the fundamental laser ablation studies toward laser desorption of calcite; a particularly stable form of calcium carbonate found in tank waste and in the earth's subsurface. We believe that LAMS studies of this material will provide much fundamental data, and will guide the soil/waste analysis work in much the same way that the sodium nitrate studies guided the tank waste investigations. We will continue to apply MALDI, in the positive and negative mass modes, to analysis of waste compounds, alone and in combination to simulate waste.

To date, all of the necessary technical tools for routine utrasensitive detection of technitium, strontium, and other radioisotopes using solid state diode lasers have been developed. In particular, SERDP funding has supported research into the external cavity control of diode lasers, laser frequency doubling using an external ring cavity, and the locking of the diode laser to an atomic resonance. Each of these individual accomplishments represents a significant advance. In addition, specific excitation schemes based on diode laser emission have been designed for technitium, strontium, plutonium, and calcium. The schemes for detection of strontium and calcium have recently been demonstrated. [12, 45, 46] It should be stressed that the compact diode laser quite likely represents the most reliable technology available for field analysis and that an applied engineering effort to design such a device should be considered.

A major goal of this SERDP program is to communicate these results to more applied analytical programs such that this fundamental knowledge can guide the approach and design of field analysis. This report is an important step toward achieving this goal. The Appendices contain a listing of the refereed publications that resulted from SERDP funding of Laser Ablation/Ionization Characterization of Solids, a partial listing of public presentations and a highlighting of the relevance of this program to DoD.

Acknowledgment: This research was supported by the Strategic Environmental Research and Development Program. Pacific Northwest National Laboratory is operated for the U.S. Department of Energy by Battelle under contract No. DE-AC06-76RLO 1830. Computer

resource allocations at the National Energy Research Supercomputer Center (Livermore, CA) were provided by the Scientific Computing Staff, Office of Energy Research Division of Chemical Sciences, Office of Basic Energy Sciences.

References

1. J.J. Shin, S.C. Langford, J.T. Dickinson and Y. Wu, *Nucl. Instrum. Meth. Phys. Rev. B* **103**, (1995).
2. M.I. McCarthy, K.I. Peterson and W.P. Hess, *J. Phys. Chem.* **100**, (1996).
3. L. McEwen, *J. Chem. Phys.* **34**, (1961).
4. A.P. Toste and R.B. Myers, *The Effects of Natural Organic Compounds and of Microorganisms on Radionuclide Transport. RWM-6 Radioactive Waste Management Committee, OECD Nuclear Energy Agency, Paris, France.* 57 (1986).
5. K. Tanaka, H. Waki, Y. Ido, S. Akita, Y. Yoshida and T. Yoshida, *Rapid Commun. Mass Spectrom* **2**, 151 (1988).
6. R.C. Beavis and J.N. Bridson, *J. Phys. D: Appl. Phys.* **26**, 442 (1993).
7. M.W. Duncan, G. Matanovic and A. Cerpa-Poljak, *Rapid Commun. Mass Spectrom.* **7**, 1090 (1993).
8. A.M. Belu, J.M. DeSimone, R.W. Linton, G.W. Lange and R.M. Friedman, *J. Am. Soc. Mass Spectrom.* **7**, 11 (1996).
9. R.C. Plumb and J.O. Edwards, *J. Phys. Chem.* **96**, 3245 (1992).
10. J.A. Campbell, K.L. Wahl, K.E. Grant, S.A. Clauss, G.M. Mong, R.B. Lucke and B.D. Lerner. *DOE Methods for Evaluating Environmental and Waste Management Samples* (1995).
11. J.A. Campbell, H.R. Udseth and R.B. Lucke. *Application of Electrospray Mass Spectrometry to the Analysis of Chelator and Chelator Fragments in Mixed Hazardous Wastes* 1-1334 (Washington D.C., 1992).
12. K. Knutsen and T.M. Orlando. *Phys. Rev. B.* **55**, 13247 (1997).
13. O. Kornienko, S. Brynjelsen, L. Hanley and T.M. Orlando. *Analysis of EDTA by laser desorption ion trap mass spectrometry* , 44th ASMS Conference of Mass Spectrometry and Allied Topics, (Portland, OR, 1996).
14. R.E. Johnson, *Intl. J. Mass Spec. Ion Processes* **139**, 25 (1994).
15. R. Levis, *Ann. Rev. Phys. Chem.* **45**, 483 (1994).
16. A.I. Gusev, W.R. Wilkinson, A. Proctor and D.M. Hercules, *Anal. Chem.* **67**, 1034 (1995).
17. H. Ehring and B.U.R. Sundqvist, *J. Mass Spec.* **30**, 1303 (1995).
18. E.R. Denoyer, N.S.J. Fredeen and J.W. Hagler, *Anal. Chem.* **63**, 445A (1991).
19. R. Lidgard and M.W. Duncan, *Rapid Commun. Mass Spectrom.* **9**, 128 (1995).
20. B.T. Chait, R. Wang, R.C. Beavis and S.B.H. Kent, *Science* **262**, 89 (1993).

21. M. Karas and F. Hillenkamp, *Anal. Chem.* **60**, 2299 (1988).

22. M. Karas, E. Nordhoff, B. Stahl, K. Strupat and F. Hillenkamp. *Matrix-Mixtures for a Superior Performance of Matrix-Assisted Laser Desorption Ionization Mass Spectrometry.* The 40th ASMS Conference on Mass Psectrometry and Allied Topics, 368 (1992).

23. J.A. Campbell, S.A. Clauss, K.E. Grant, V. Hoopes, B.D. Lerner, R.B. Lucke, G.M. Mong, J. Rau and R. Steele. *Flammable Gas Safety Program, Analyical Methods Development: FY 1993 Progress Report* (Pacific Northwest Laboratory, Richland, Washington., 1993).

24. J.A. Campbell, S.M. Stromatt, D.W. Koppenaal, R.M. Bean, T.E. Jones, D.M. Strachan and H. Babad, *Anal. Chem.* **66**, 1208A (1994).

25. B.A. Bushaw, H.J. Kluge, J. Lantzsch, R. Schwalbach, J. Stenner, H. Stevens, K. Wendt and K. Zimmer, *Z. Phys. D* **28**, (1993).

26. P.C. Liao and J. Allison, *J. Mass Spec.* **30**, 408 (1995).

27. C.A. Brau, *Science* **39**, 1115 (1988).

28. W.P. Hess, H.K. Park, O. Yavas and R.F. Haglund Jr., *App. Surf. Sci.* (in press) (1998).

29. R.A. Bradley, E. Lanzendorf, M.I. McCarthy, T.M. Orlando and W.P. Hess, *J. Phys. Chem.* **99**, 11715 (1995).

30. A.I. Gusev, W.R. Wilkinson, A. Proctor and D.M. Hercules, *Anal. Chem.* **67**, 1034 (1995).

31. C.A. Brau, Free-Electron Lasers, Academic Press, Boston (1990).

32. K.L. Busch, *J. Mass Spectrom.* **30**, 233 (1995).

33. Y. Yang and R. Orlando, *Anal. Chem.* **68**, (1996).

34. K. Strupat, M. Karas and F. Hillenkamp, *Intl. J. Mass Spec. Ion Processes* **111**, 89 (1991).

35. R.A. Bradley, E. Lanzendorf, M.I. McCarthy, T.M. Orlando and W.P. Hess, *J. Phys. Chem.* **99**, 11715 (1995).

36. C.E. Weiman and L. Hollberg, *Rev. Sci. Instrum.* **62**, (1991).

37. E.W. Schlag, J. Grotemeyer and R.D. Levine, *Chem. Phys. Lett.* **190**, 521 (1992).

38. H. Yamashita, *J. Phys. Soc.* **33**, 1407 (1972).

39. J.L. Means, D.A. Crerar and J.O. Duguid, *Science* **200**, 1477 (1978).

40. D.J. Harvey, *Rapid Commun. Mass Spectrom.* **7**, 614 (1993).

41. P. Martin, S. Guizard, P. Daguzan, G. Petite, P. D'Oliveria, P. Meynadier and M. Perdix, *Phys. Rev. B.* **55**, 5799 (1997).

42. E. Tokunaga, A. Terasaki and T. Kobayashi, *Opt. Lett.* **17**, 1131 (1992).

43. E. Tokunaga, A. Terasaki and T. Kobayashi, *J. Opt. Soc. Am. B* **12**, 753 (1995).

44. A. Westman, T. Huth-Fehre, P. Demirev and B.U.R. Sundqvist, *J. Mass Spec.* **30**, 206 (1995).

45. M.L. Alexander, P.H. Hemberger, M.E. Cisper and N. Nogar, *Anal. Chem.* **65**, 1609 (1993).

46. J.A. Campbell, R.B. Lucke and S.A. Clauss. *Application of LC/MS to the Study of Chelators in Mixed Hazardous Wastes* 1334, 35th ASMS Conference on Mass Spectrometry and Allied Topics, (Nashville, Tennessee, 1991).

Appendix A: List of publications resulting from SERDP supported work.

K. M. Beck, D. P. Taylor, and W. P. Hess, "Photostimulated Desorption of CO from Geologic Calcite Following 193 nm Irradiation," Phys. Rev. B. **55**, 13253 (1997).

S. C. Goheen, K. L. Wahl, J. A. Campbell, and W. P. Hess, "Mass Spectrometry of Low Molecular Weight Solids by Matrix-Assisted Laser Desorption /Ionization," J. Mass Spectrom. **32**, 820 (1997).

K. M. Beck, M. I. McCarthy, and W. P. Hess, "Atomic and Molecular Photostimulated Desorption from Complex Ionic Crystals." J. Electron. Materials, **26**, 1335 (1997).

W. P. Hess, H. K. Park, O. Yavas, and R. F. Haglund, Jr., "IR MALDI of Low Molecular Weight Compounds Using a Free-Electron Laser," Appl. Surf. Sci. (in press).

K. M. Beck and W. P. Hess, "Quantum-State Resolved Products via Vacuum Ultraviolet Photostimulated Desorption from Geologic Calcite," Appl. Surf. Sci. (in press).

R. A. Bradley, Jr., E. Lanzendorf, M. I. McCarthy, K. Peterson, T. M. Orlando, and W. P. Hess. "Molecular NO Desorption From Crystalline Sodium Nitrate by Resonant Excitation of the π-π^* Transition." *J. Phys. Chem.* 99, 11715, (1995).

W. P. Hess, B. A. Bushaw, M. I. McCarthy, J. A. Campbell, S. D. Colson, and J. T. Dickinson, "Laser Ablation/Ionization Characterization of Solids: Interim Progress Report of the Strategic Environmental Research Development Program." (January, 1996)

Wayne P. Hess, Kristine A. H. German, Richard A. Bradley, and Maureen I. McCarthy. "Laser Ablation of Sodium Nitrate: NO Desorption Following Excitation of the π–π^* Band of the Nitrate Anion." Appl. Surf. Sci. 96-98, 321 (1996).

M. I. McCarthy, K. Peterson, and W. P. Hess. "Electronic Structure of Sodium Nitrate: Investigations of Laser Desorption Mechanisms." J. Phys. Chem. 100, 6708, (1996).

Kenneth M. Beck , Kristine A. H. German , and Wayne P. Hess, "Thermal Distributions Deduced from (2+1) Resonance Enhanced Multiphoton Ionization of CO Products." Chem. Phys. Lett. 256, 297, (1996).

D. R. Ermer, J.-J. Shin, S. C. Langford, and J. T. Dickinson, Positive ion emission accompanying uv irradiation of single crystal MgO and NaNO3, to appear in Advanced Laser Procesing of Materials-Fundamentals and Applications, edited by R. K. Singh, D. Norton, J. Narayan, J. Cheung, and L. D. Laude, MRS Symp. Proc. 397 (Materials Research Society, Pittsburg, Pennsylvania, 1996).

J. T. Dickinson, J.-J. Shin, and S. C. Langford, "The role of defects in laser induced positive ion emission from ionic crystals," Appl. Surf. Sci. 96-98, 316-320 (1996).

J. T. Dickinson, J. J. Shin, and S. C. Langford, "Laser-induced emission of neutral atoms and molecules from electron-irradiated NaNO3," Appl. Surf. Sci. 96-98, 326-331 (1996).

D. R. Ermer, J.-J. Shin, S. C. Langford, K. W. Hipps, and J. T. Dickinson, "Interaction of wide band gap single crystals with 248 nm excimer laser radiation. IV. Positive ion emission from MgO and NaNO3," J. Appl. Phys. 80(11), 6452-6465 (1996).

R. L. Webb, G. Exarhos, J. T. Dickinson, "Characterization of particulates generated from laser ablation of single crystals of NaNO3,"Appl. Spectroscopy 51(5) 1997.

J.-J. Shin, D. R. Ermer, S. C. Langford, and J. T. Dickinson, "The role of photoelectronic processes in the formation of a fluorescent plume on single crystal NaNO3 by 248-nm laser irradiation," Appl. Phys. A 64, 7-18 (1997).

J. J. Shin, Myoung-Won Kim, and J. T. Dickinson, "Effect of tribological wear on UV laser interactions with single crystal NaNO3 and CaCO3," J. Appl. Phys. 80, 7065-7072 (1996).

R. L. Webb and J. T. Dickinson, "The role of defects in the rear side laser ablation of MgO at 308 nm," J. Appl. Phys. 80, 7057-7064 (1996).

D. R. Ermer, S. C. Langford, and J. T. Dickinson, "Interaction of wide band gap single crystals with 248 nm excimer laser radiation. V. The role of photoelectronic processes in the formation of a fluorescent plume from MgO," J. Appl. Phys. 81(3) 1495-1504 (1997).

S. C. Langford and J. T. Dickinson, "Applications and mechanisms of laser ablation for elemental analysis of nuclear waste and contaminated soils," Advanced Technologies for Environmental Monitoring and Remediation, SPIE Proceedings Vol. 2835, edited by Tuan Vo-Dinh (SPIE: The International Society for Optical Engineering, Bellingham, Washington, 1997), pp. 62-72.

J. T. Dickinson, D. R. Ermer, J. J. Shin, and S. C. Langford, "A defect-mediated multiple-photon mechanism for ion emission from ionic materials under UV laser irradiation," in Defects in Insulating Materials, Mater. Sci. Forum Vol. 239-241, edited by G. E. Matthews and R. T. Williams (Trans Tech Publications, Switzerland, 1997), pp. 641-646.

J. T. Dickinson, "Low Fluence Laser Desorption and Plume Formation from Wide Bandgap Crystalline Materials", in Laser Ablation and Desorption, Vol 30 Experimental Methods in the Physical Sciences, J. C. Miller and R. F. Haglund, eds. (Academic Press, 1998, New York), pp. 139-172.

J. T. Dickinson, D. R. Ermer, J.-J. Shin, and S. C. Langford, "Desorption of positive ions and plume formation from laser irradiation of ionic crystals," in Laser Applications in Microelectronic and Optoelectronic Manufacturing II SPIE Proceedings Volume 2991, edited by J J Dubowski, (SPIE: The International Society for Optical Engineering, Bellingham, Washington, 1997).

J. T. Dickinson, D. R. Ermer, J.-J. Shin, and S. C. Langford, "The Dynamics of laser induced particle emission and plume formation from wide bandgap materials,". to appear in Appl. Surf. Sci.

S. C. Langford, M. L. Dawes, and J. T. Dickinson, "The Role of Dehydration in excimer laser interactions with a transparent, hydrated mineral-CaHPO4.2H2O," to appear in Appl. Surf. Sci.

D. R. Ermer, J. T. Dickinson, and S. C. Langford, "Electrostatic Expansion of a laser-induced plasma formed from MgO during irradiation at 248 nm," to appear in Appl. Surf. Sci.

T. Lippert, J. T. Dickinson, S. C. Langford, H. Furutani, H. Fukumura, and H. Mashuhara, "Photopolymers designed for laser ablation photochemical ablation mechanism", to appear in Appl. Surf. Sci.

R. L. Webb, T. Lippert, S. C. Langford, and J. T. Dickinson, "Sensitization of PMMA to excimer laser ablation at 308 nm wavelength," to appear in Appl. Surf. Sci.

R. Webb, J. T. Dickinson, and S. C. Langford, "Neutral Atom and Molecule Emission Accompanying 248-nm Laser Irradiation of Single Crystal $NaNO_3$."*Nucl. Instrum. Meth. Phys. Rev. B* . 103, 297, (1995).

J.-J. Shin, S.C. Langford, J. T. Dickinson, and Y. Wu "Electron Stimulated Neutral and Ion Emission from Single Crystal $NaNO_3$."*Nucl. Instrum. Meth. Phys. Rev. B* . 103, 284, (1995).

S. C. Langford and J. T. Dickinson, "Applications and Mechanisms of Laser Ablation for Elemental Analysis of nuclear Wastes and Contaminated Soils." SPIE Manuscript 2835-20 p.1. 1996, SPIE Meeting Denver, CO.

B. A. Bushaw, H.-J. Kluge, J. Lantzsch, R. Schwalbach, J. Stenner, H. Stevens, K. Wendt, and K. Zimmer, "Hyperfine Structure in 5s4d ^3D - 5snf Transitions of ^{87}Sr." Z. Phys. D 28, 275-281 (1993).

K. Zimmer, J. Stenner, H.-J. Kluge, J. Lantzsch, L. Monz, E.W. Otten, G. Passler, R. Schwalbach, M. Schwarz, H. Stevens, K. Wendt, G. Herrmann, S. Niess, N. Trautmann, K. Walter, and B. A. Bushaw, "Determination of ^{90}Sr in Environmental Samples with Resonance Ionization Spectroscopy in Collinear Geometry," Appl. Phys. B 59, 117-121 (1994)

H.-J. Kluge, B. A. Bushaw, G. Passler, K. Wendt, N. Trautmann, "Resonance ionization spectroscopy for trace analysis and fundamental research," Fresenius J. Anal. Chem. 350, 323-329 (1994).

J. Lantzsch, B. A. Bushaw, G. Herrmann, H.-J. Kluge, L. Monz, S. Niess, E. W. Otten, R. Schwalbach, M. Schwarz, J. Stenner, N. Trautmann, K. Walter, K. Wendt, K. Zimmer,

"Trace analysis of the Radionuclides ^{90}Sr and ^{89}Sr in environmental samples I: Laser Mass Spectrometry," Angew. Chem. Int. Ed. Engl. 34, 181-183 (1995).

J. Lantzsch, B. A. Bushaw, V. A. Bystrow, G. Herrmann, H.-J. Kluge, S. Niess, E. W. Otten, G. Passler, R. Schwalbach, M. Schwarz, J. Stenner, N. Trautmann, K. Wendt, Y. V. Yushkevich, K. Zimmer, "Trace determination of ^{90}Sr and ^{89}Sr in environmental samples by collinear resonance ionization spectroscopy," AIP Conf. Ser. 329 (RIS 94), H.-J. Kluge, J. E. Parks, K. Wendt, Eds., 251-254 (1995).

B. A. Bushaw, H.-J. Kluge, J. Lantzsch, R. Schwalbach, M. Schwarz, J. Stenner, H. Stevens, K. Wendt, K. Zimmer, "Hyperfine structure of $^{87,89}Sr$ $4s4d\,^3D$ - 5snf transtions in collinear fast beam RIMS," AIP Conf. Ser. 329 (RIS 94), H.-J. Kluge, J. E. Parks, K. Wendt, Eds., 381-384 (1995).

Appendix A: List of Selected Presentations

Los Alamos National Laboratory, Los Alamos, NM January, 1997. "Laser Desorption in Molecular Speciation."

American Chemical Society National Meeting, San Francisco, CA, April, 1997. "Molecular Desorption from Ionic Molecular Crystals following Resonant UV Excitation."

American Chemical Society National Meeting, San Francisco, CA, April, 1997. "Development of laser ablation for characterization of hazardous waste and contaminated soils."

Conference on Laser Ablation, COLA '97, Pacific Grove, CA July, 1997. "IR MALDI of Low Molecular Weight Compounds Using a Free-Electron Laser."

BES Program Review Richland, WA, "Energetic Processes Program." February 1997.

SERDP Program Review Alexandria, VA, "Laser Ablation/Ionization Characterization of Solids." May 1997.

American Vacuum Society Pacific Northwest Meeting, Troutdale, OR September, 1997. "Photostimulated Desorption from Molecular Ionic Crystals Following Resonant UV Laser Excitation."

IEEE/LEOS 1996 Summer Topical Meetings, Keystone, CO August 5-9, 1996, "Laser Desorption of NO and CO from Sodium Nitrate and Calcium Carbonate Crystals." Presented by W. P. Hess.

Gordon Research Conference on Laser Interacions with Materials, Holderness, New Hampshire, June 9-14, 1996. Molecular Desorption from Ionic Molecular Crystals Following Resonant UV Excitation." Presented by W. P. Hess.

"Laser Ablation of Sodium Nitrate in the 6 eV Band." Physical Chemistry Seminar, Weizmann Institute of Science, Rehovot, Israel, June 1994. Presented by W. P. Hess.

"Laser Ablation of Sodium Nitrate in the 6 eV Band." Physical Chemistry Seminar, Hebrew University, Jerusalem, Israel, June 1994. Presented by W. P. Hess.

"Laser Interactions with an Ionic Molecular Crystal : Sodium Nitrate Ablation in the 6 eV Valence Band." Gordon Conference on Laser Surface Interactions, Colby-Sawyer College, New London, New Hampshire, August, 1994. Presented by W. P. Hess.

"Laser Ablation/Ionization Characterization of Solids." Strategic Environmetal Research Development Program Symposium, Washington D.C., April, 1995. Presented by W. P. Hess.

"Laser Ablation of Sodium Nitrate: NO Desorption Following Excitation of the π–π^* Band of the Nitrate Anion." European Materials Research Society Spring Meeting, Symposium F, Conference on Laser Ablation, Strasbourg, France May, 1995. Presented by W. P. Hess.

"Molecular NO Desorption from Sodium Nitrate by Resonant Excitation of a π-π^* transition on NO_3 Anion." American Chemical Society Regional Meeting, Park City, Utah, June, 1995. Presented by W. P. Hess.

"Laser ionization Probing of Molecular Product State Distributions: Photodissociation of Isolated Molecules and Photdesorption from Ionic Crystals." Physiscs Deparment Coloquium, Washington State University, Pullman, Washington, Spetember 1995. Presented by W. P. Hess.

"Laser Desorption from Resonant Excitation of Molecular Ionic Crystals." Chemistry Deparment Coloquium, Colorado State University, Fort Collins, Colorado, Spetember 1995. Presented by W. P. Hess.

"Laser Desorption from Resonant Excitation of Molecular Ionic Crystals." Chemical Physics Coloquium, University of Colorado, Boulder Colorado, September 1995. Presented by W. P. Hess.

"Matrix-Assisted Laser Desorption Ionization-TOF of Low Molecular Weight Organics." American Society of Mass Spectrometry Meeting, Portland, Oregon, May 1996. Presented by J.A. Campbell.

"Excimer Laser Interactions with Wide Bandgap Materials," Freie Universitat, Berlin, Germany, June, 1994. Presented by J. T. Dickinson.

"Laser Desorption and Ablation of Wide Bandgap Materials," Gordon Conference on Laser-Materials Interactions, August, 1994. Presented by J. T. Dickinson.

"Laser Desorption of Ions and Neutrals from Ionic Crystals," Physics Department, U. of Osaka, Osaka, Japan, January 1995. Presented by J. T. Dickinson.

"Excimer laser interactions with single crystal NaNO3," American Vacuum Society PNW Meeting, Portland, September, 1994. Presented by J. T. Dickinson.

"Laser Induced Positive Ion Emission and Laser Ablation from single crystal NaNO3," American Vacuum Society PNW Meeting, Portland, September, 1994. Presented by J. T. Dickinson.

"The role of defects in the laser induced decomposition of NaNO3," Conference on Laser Ablation, Strasbourg, France, May, 1995. Presented by J. T. Dickinson.

"Applications and Mechanisms of laser ablation for elemental analysis of nuclear wastes and contaminated soil," MRS Fall Meeting, Boston, Nov. 1995. Presented by J. T. Dickinson.

"Strontium 90 detection by collinear beam spectroscopy", University of Bern, Bern, Switzerland, June 28, 1993. Presented by B. A. Bushaw.

"Perturbed Hyperfine Structure in 5s4d ^{3}D - 5snf Transitions of ^{87}Sr," 25th annual conference of the European Group for Atomic Spectroscopy, Caen, France, July 13, 1993. Presented by B. A. Bushaw.

"Rare Isotope Analysis with cw-RIMS", Gesellschaft fuer Schwerionforschung (GSI), Darmstadt, Germany, Oct. 20, 1993. Presented by B. A. Bushaw.

Appendix B: Relevance to the Department of Defense

The Laser Ablation/Ionization Characterization of Solids program has been funded under the compliance pillar of the SERDP program. While many application of our SERDP efforts directly impact DOE hazardous and mixed waste clean-up it was agreed at the SERDP In Process Review (May, 1996), that this report should comment upon program relevance to DoD to encourage greater mission connection and promote follow-on funding. As suggested by Dr. John Harrison, Dr. Wayne Hess contacted Dr. John Cullinane of the US Army Waterways Experiment Station. A summary of program results and reports have been sent to Dr. Cullinane and Dr. Cullinane has agreed to distribute these reports to the appropriate technical contacts to increase visibility of the Laser Ablation/Ionization Characterization of Solids program to possible DoD end users.

There are distinct scenarios for the application of Laser Ablation/Ionization Characterization technology. The most obvious scenario involves monitoring environmental cleanup in friendly areas. Direct reductions of expense and task completion time result when the clean-up contractor knows the identity and quantity of materials to be removed. The DoD has an extensive list of such contaminated sites which will require methods for determining end state cleanliness. Examples of contamination includes spills of hydrocarbons, polychlorinated biphenyls and other carcinogens, lead, and mercury. Soil contamination at firing range sites may require, in excess of removal of unexploded ordinance, soil analysis, again to verify a clean end state. Numerous contaminated DoD sites such as the Rocky Mountain Arsenal, could likely make use of a field deployable analytical instrument based on the techniques developed in this program.

A second scenario involves monitoring unfriendlies for chemical weapons (CW) and nuclear proliferation (NP). We have submitted proposals for the development of a compact, rugged, field-deployable analytical systems for environmental monitoring. Such a system could provide rapid detection of chemical agents under battlefield conditions. The sensitivity to solid species could verify chemical agent use via detection of even minor soil contamination long after the fact. The development of diode laser technology has been rapid in recent years due to their immense commercial impact. As a consequence of this development, device reliability, power, wavelength range and tunability have improved dramatically. Efforts under the Laser Ablation/Ionization Characterization of Solids program indicate that a device capable of extreme sensitivity (femtogram level) for technetium or other fission products could be constructed. While this report has described the environmental impact of technetium release from plutonium production facilities, it has not mentioned that technetium has near zero background in nature (it is only produced by cosmic ray impact of molybdenum and can only be found in molybdenum rich ore). Therefor technetium is nearly exclusively produced by fission. Hence its presence can be a strong indication of nuclear weapons production. The diode laser ionization schemes described within this report are capable of detecting the most minute concentrations of radioisotopes. Extremely little sample is required to construct an accurate picture of nuclear activity and capabilities. A third obvious scenario involves cooperative monitoring for treaty verification with respect to NP and CW. The advantages over existing technology are the extreme sensitivity of the diode laser approach and the rapid analysis of solids for the LAMS approach.